scientific reports

Check for updates

OPEN

# Synthesis, biological evaluation, and molecular docking of novel coumarin-based bisimine derivatives

Atieh Abazari[1], Yaghoub Sarrafi, Pouya Taheri[1]✉ & Mahmood Tajbakhsh[1]

**Schiff bases derived from 3-acetyl-4-hydroxycoumarin represent a promising yet underexplored scaffold in medicinal chemistry. Here, we report the efficient synthesis of a series of bisimine derivatives (3a–j) through condensation with structurally diverse amines, achieving yields of 68–95%. Spectroscopic characterization (NMR, IR, MS) confirmed their unique architectures, with 3j emerging as a standout candidate exhibiting anticancer activity comparable to doxorubicin but with superior selectivity against MCF-7 and A549 cell lines. Among the tested derivatives, compound 3a exhibited the most potent antibacterial activity, with the lowest MIC values observed against Gram-positive strains. Notably, 3f (a thiourea analog) demonstrated broad-spectrum antifungal efficacy (MICs: 1.95–31.25 µg/mL), while 3c surpassed ascorbic acid in radical scavenging (96.7% DPPH inhibition). Molecular docking revealed robust interactions between lead compounds (3b, 3c, 3j) and key therapeutic targets (FGFR1, cIAP1-BIR3), suggesting a dual inhibitory mechanism. These findings underscore the potential of coumarin bisimines as versatile platforms for addressing antibiotic resistance and oxidative stress-related pathologies.**

**Keywords** Schiff base, 4-Hydroxycoumarin, Antibacterial, Cancer therapeutics, Molecular docking

In recent years, an increase in infectious diseases brought on by bacteria and fungi has threatened human health[1]. Despite the availability of several antibiotics, multidrug resistance (MDR) has emerged among the majority of pathogenic bacteria[2]. To unravel these problems posed by antibiotic-resistant bacteria, novel antibacterial drugs are being proposed that are more effective than those currently available against such bacteria. It emphasizes the importance of exploiting upcoming medications with antimicrobial and antioxidative capabilities that are expected to prevent and treat illnesses more effectively. The present research describes novel synthetic 3-acetyl-4-hydroxycoumarin Schiff bases exhibiting significant antimicrobial and antioxidant activity.

Coumarin (2 H-chromen-2-one or 2 H-1-benzopyran-2-one) has a benzene ring and a 2-pyrone ring that are joined together. There have been reports of coumarin compounds being detected in microorganisms, animals, essential oils, and fruits[3,4]. To date, a total of 800 coumarin derivatives have been found in nature[5]. Natural and synthetic coumarins exhibit various biological and therapeutic potentials, such as anti-inflammatory[6], anti-oxidant[7], antibacterial[8] and anti-carcinogenic effects[9]. For example, 4-hydroxycoumarin exhibits anticoagulant effects by antagonizing vitamin K[10]. Several derivatives of coumarin are capable of inhibiting cell proliferation, including 4-hydroxycoumarin analogs and their complexes[11,12]. This is because 4-hydroxycoumarins interact with enzymes involved in the cell cycle, such as DNA polymerase and topoisomerase. By blocking these enzymes, cell proliferation is inhibited[13].

4-Hydroxycoumarins have drawn significant interest because of their biological properties and distinctive molecular structure. These compounds exhibit a range of pharmacological effects, including antibacterial and antiviral activities, antioxidant properties, allergy prevention, anti-inflammatory, and even potential anti-cancer properties[14].

In the context of ongoing research into the preparation of coumarin derivatives, in particular, 4-hydroxycoumarin derivatives possess antibacterial and antioxidant activities[15]. 3-acetyl-4-hydroxycoumarin can be considered the fundamental framework of numerous natural substances and is used as the primary pharmacophore in various medicinal compounds, including antimicrobial, antifungal, and antioxidant agents[16]. Due to its remarkable properties, 3-acetyl-4-hydroxycoumarin is a desirable target for organic chemists,

[1]Department of Organic Chemistry, University of Mazandaran, Babolsar, Mazandaran, Iran. ✉email: pooyataheri90@yahoo.com

and several approaches have been developed to synthesize this compound, namely acylation, bromination, metalation, and Claisen-Schmidt condensation. Furthermore, its versatile nature enables the synthesis of several derivatives of 3-acetyl-4-hydroxycoumarin, which are essential to expanding research in organic chemistry.

The carbon-nitrogen double bond (-C = N-), i.e., Schiff base, plays a significant role in chemical reactions. This functional group has made remarkable contributions to scientific advancement[17]. Schiff bases are utilized as intermediates for synthesizing many pharmaceutical substances[18]. Schiff bases having different heterocyclic scaffolds, e.g., pyrazole, coumarin, etc., show many biological and pharmacological characteristics, including antimicrobial[19], antibacterial[20], anti-inflammatory and analgesic[21], anti-tuberculosis[22], antifungal[23], anticancer[24], antioxidant[25], cytotoxic[26], and many other pharmacological activities.

Numerous studies[24,27] have suggested the development of anticancer agents based on 3-substituted chromones and coumarins. Particularly, Schiff bases of 3-substituted coumarins possess antioxidant[28], antifungal[29] and anticancer[30] properties. A sequence of sulfonamide-based coumarin Schiff bases were synthesized and evaluated for their potential as cytotoxic agents in two different cell lines, namely MCF-7 (breast cancer) and B16-F10 (B16 melanoma)[31]. Additionally, coumarin Schiff bases derived from phosphorohydrazine act as alkylating agents targeting leukemia cell lines P388 and L1210[32,33].

This research boards on the innovative journey of synthesizing 3-acetyl-4-hydroxycoumarin bisimines derivatives, leveraging an array of primary amines including hydrazine, diethylenetriamines, triethylenetetramine, urea, thio urea, guanidine, semi-carbazide, 1,2-diaminocyclohexane, 2,3-diaminopyridine, and melamine.

To date, previously reported Schiff bases derived from coumarins demonstrated moderate activity in antibacterial and anticancer studies but were often hindered by issues such as low selectivity, limited functional diversity, and suboptimal binding affinities. For example, studies on coumarin-based Schiff bases have reported activity against limited bacterial strains or cancer cell lines, without a broad-spectrum evaluation or an exploration of molecular interactions. Many derivatives were also limited to monoamine reactions, lacking the complex structural designs achievable through bisimine formation.

A study by Patil et al. focused on coumarin Schiff bases but found moderate antibacterial activity primarily against E. coli and S. typhi, with limited spectrum coverage and no molecular insights provided[34].

Kumar et al. noted poor receptor binding in coumarin-based anticancer agents, limiting their efficacy against cancer cell lines like MCF-7 and A549[36].

A key distinction between this work and previous studies lies in the incorporation of diverse diamine reactants to form symmetric and asymmetric bisimines, which expand the functional scope of these compounds. Earlier studies often employed monoamine reactions that limited structural complexity and biological applications. For example, comparable Schiff base derivatives reported by Erturk et al. (2020) focused entirely on antibacterial properties without addressing antifungal or antioxidant potential[36]. Moreover, research by Kalaiarasi et al. (2019) highlighted coumarin Schiff bases but noted limited anticancer activity due to poor receptor binding[35].

In contrast, our derivatives, exhibit superior receptor interactions and broader activity profiles, as demonstrated through molecular docking and bioassays. These advancements underscore the potential of bisimine-based coumarins as multifunctional therapeutic agents, addressing a broader range of biomedical challenges. The complex and costly synthesis processes involved in creating bisimines further impede their widespread use and development.

To address these gaps in the existing literature, this study aims to overcome these challenges by synthesizing novel symmetric and asymmetric bisimines using a diverse range of amines. The resulting Schiff bases underwent comprehensive in-vitro biological assays, including antibacterial, antioxidant, antifungal, and cytotoxicity tests, to evaluate their biological activity. The synthesized compounds exhibited high synthetic efficiency and promising biological responses, highlighting their potential therapeutic applications. Advanced spectroscopic techniques, such as FT-IR, NMR, mass spectrometry, and elemental analysis, were employed to confirm the structure of the Schiff bases, ensuring the reliability of the results. In addition to the synthesis and biological evaluation of novel symmetric and asymmetric bisimines, this study further explored the interaction between the synthesized compounds and target proteins through molecular docking. This approach leverages the predictive power of molecular docking to provide insights into the ligand-receptor interactions, offering a deeper understanding of the compounds' potential therapeutic efficacy.

These findings suggest promising opportunities for future drug development, emphasizing the importance of addressing the limitations in current imine research.

## Experimental

### Materials and methods

This experiment used highly pure chemicals and reagents from Sigma-Aldrich Chemical Company (St. Louis, MO) and Merck Laboratory Supplies (Darmstadt, Germany). Using a Perkin-Elmer spectrum, infrared spectra were captured based on a KBr pellet spectrometer (4000 –400 $cm^{-1}$). $^{1}H$ and $^{13}C$ NMR spectra were acquired through a Bruker DRX-400 (400 MHz) spectrometer in DMSO-d6 as a solvent and using tetramethylsilane as an internal standard. ElectroThermal 9100 apparatus was used to determine the melting point. Mass spectra were obtained using a Finnigan-MAT 8430 GC-MS system with an electron ionization source operated at 70 eV. An HP-5MS capillary column (30 m x 0.25 mm i.d, 0.25 micron film) was used for chromatographic separation with helium as the carrier gas at a flow rate of 1.0 mL/min. The oven temperature program was as follows: an initial hold 70 °C for 2 min, ramped at 10 °C/min to 280 °C, and held for 5 min. Injector temperature was maintained at 250 °C with a splitless mode of injection. The mass scan range was m/z 40–600 and spectra were taken in full-scan mode.

### Preparation of 3-acetyl-4-hydroxy-2*H*-chromene-2-one (2)

A literature-reported method was used to prepare compound **2**[37]. Typically, 4-hydroxy-2 H-chromene-2-one (0.81 g, 5 mmol) (1) was dissolved in acetic acid (5.5 mL) and then phosphorus oxychloride ($POCl_3$) (1.5 mL) was added dropwise at ambient temperature. To obtain favorable yields of the desired product, the reaction mixture was conducted at reflux conditions for 30 min. Then an additional volume of $POCl_3$ (1 mL) was injected into the solution. Subsequently, the solution was agitated under reflux for half an hour. Upon cooling, the resulting product was obtained as an orange powder. The reaction was monitored by thin-layer chromatography (TLC). Recrystallization with EtOH was performed to purify the product. This resulted in white needle-like crystals of pure compound **2**. The desired product was identified by $^1H$ and$^{13}C$ NMR and FT-IR spectroscopy. (Yield = 0.19 g, 94%.

**m.p.**: 134–136 °C (135–136 °C [38]); **IR** ($\upsilon_{max,}$ $cm^{-1}$): (OH): 3455, ($C_{Ar}H$): 3154, ($C_{SP}{}^3$-H): 2924, (C = O): 1746, 1722, (C = C): 1616, (C = $C_{Aryl}$): 1556, 1465. **Mass analysis**: 204.4 $g.mol^{-1}$. **$^1$H NMR** (400 MHz, DMSO-d6) δH: 2.61 (*s*, 3H, $CH_3$), 7.34 (*d*, 1 H, $^3J_{HH}$= 8.4 Hz, $H_{Ar}$), 7.39 (*td*, 1 H, $^3J_{HH}$= 8.4, $^4J_{HH}$: 0.8 Hz, $H_{Ar}$), 7.78 (*td*, 1 H, $^3J_{HH}$= 8.8, $^4J_{HH}$: 1.6 Hz, $H_{Ar}$), 7.94 (*dd*, 1 H, $^3J_{HH}$= 8.8, $^4J_{HH}$: 1.6 Hz, $H_{Ar}$), 17.34 (*s*, 1 H, OH). **$^{13}$C NMR** (100 MHz, DMSO-d6) δ: 30.03, 101.70, 115.18, 117.16, 125.26, 125.64, 137.12, 154.46, 159.82, 178.32, 205.96.

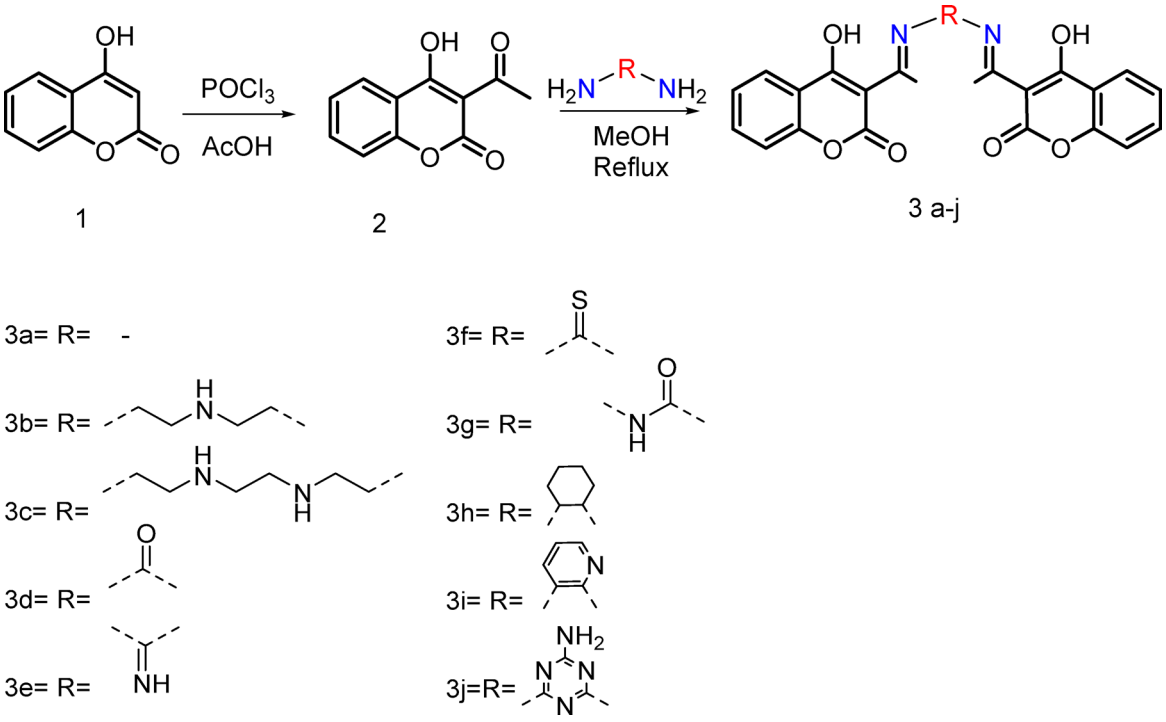
*General procedure for synthesizing compounds (3a-j)*

A mixture of 3-acetyl-4-hydroxycoumarin **2** (2 mmol) and diamine (1 mmol) was dissolved in MeOH (10 mL) at 65 °C and refluxed for several hours using a magnetic stirrer. Reaction progression was monitored by TLC using the appropriate ratio of ethyl acetate and n-hexane solvents. After completion of the reaction, the mixture was cooled to room temperature and filtered to give the crude product. Using different purification methods such as recrystallization and solvent purification, products (3a-j) were purified and collected in either powder or crystal forms. The synthetic pathway for the preparation of compounds 3a–j is demonstrated in Scheme 1.

*Preparation and characterization of 3,3'-((1E,1'E)-hydrazine-1,2-diylidenebis(ethan-1-yl-1-ylidene))bis(4-hydroxy-2 H-chromene-2-one) [3a]*

A solution of hydrazine hydrate (0.03 mL, 0.03 g, 1.0 mmol) was added dropwise to a hot (65 °C) solution of 3-acetyl-4-hydroxycoumarin (0.408 g, 2.0 mmol) dissolved in absolute MeOH (10 mL) and agitated for 1 h. Grey precipitation was obtained and washed with cold EtOH and distilled water. Recrystallization from EtOH was used as the final purification process (Yield = 0.343 g, 85%).

**m.p.**: 221–224 °C; **Elemental analysis** for $C_{22}H_{16}N_2O_6$: **Found**: C: 65.31, H: 4.02, N: 6.89; **Calculated**: C: 65.35, H: 3.99, N: 6.93; **IR** ($\upsilon_{max}$, $cm^{-1}$): (OH): 3275, ($C_{Ar}H$): 3066, ($C_{SP}{}^3$-H): 2921, (C = O): 1733, (C = N): 1694, (C = C): 1608, (C = $C_{Aryl}$): 1557, 1461. **Mass**, m/z (%): Molecular ion: 404.10 ($M.^+$, 7.1), base peak: 202($M.^+$ -202, 100). **$^1$H NMR** (400 MHz, DMSO-d6) δH: 2.58 (*s*, 3H, $CH_3$), 7.25 (*d*, 1 H, $^3J_{HH}$= 8.4 Hz, $H_{Ar}$), 7.29 (*t*, 1 H, $^3J_{HH}$= 7.2 Hz, $H_{Ar}$), 7.63 (*td*, 1 H, $^3J_{HH}$= 8.4, $^4J_{HH}$: 1.2 Hz, $H_{Ar}$), 7.94 (*dd*, 1 H, $^3J_{HH}$= 7.6, $^4J_{HH}$: 1.6 Hz, $H_{Ar}$), 12.04 (*brs*, 1 H, OH). **$^{13}$C NMR** (100 MHz, DMSO-d6) δ: 21.4, 112.1, 121.4, 127.7, 128.5, 130.0, 136.7, 142.6, 148.6, 151.9, 153.9.




**Scheme 1**. Synthesis of 3-acetyl-4-hydroxycoumarin-derived Schiff bases.

*Preparation and characterization of 3,3'-((1E,1'E)-((azanediylbis(ethane-2,1-diyl))bis(azanylylidene))bis(ethan-1-yl-1-ylidene))bis(4-hydroxy-2 H-chromene-2-one) [3b]*

Compound **3b** was obtained after adding diethylenetriamine (0.103 gr, 1.0 mmol) to 10 mL of the mixture of absolute MeOH containing 3-acetyl-4-hydroxycoumarin (0.408 g, 2.0 mmol). Following this, the reaction mixture underwent refluxing for 1 h at 65 °C. After cooling down the solution, the white powder was collected and washed with cold EtOH repeatedly and then dried in an oven. (Yield = 0.45 g, 95%,).

**m.p.**: 188–190 °C; **Elemental analysis** for $C_{26}H_{25}N_3O_6$: **Found**: C: 65.71, H: 5.34, N: 8.80; **Calculated**: C: 65.68, H: 5.30, N: 8.84; **IR** ($\upsilon_{max}$, $cm^{-1}$): (OH): 3282, (NH): 3248, ($C_{Ar}H$): 3070, ($C_{SP}{}^3$-H): 2927, (C = O): 1730, (C = N): 1648, (C = C): 1608, 1526, (C = $C_{Aryl}$): 1456. **Mass**, m/z (%): Molecular ion: 475.17 ($M.^+$, 8.3), base peak: 273 (M-202, 100). **$^1$H NMR** (400 MHz, DMSO-d6) δH: 1.59 (*brs*, 0.5 H, NH), 2.64 (*s*, 3H, $CH_3$), 2.91 (*t*, 2 H, $^3J_{HH}$= 6.0 Hz, $CH_2$), 3.66 (*t*, 2 H, $^3J_{HH}$= 6.0 Hz, $CH_2$), 7.10 (*d*, 1 H, $^3J_{HH}$= 8.4 Hz, $H_{Ar}$), 7.14 (*t*, 1 H, $^3J_{HH}$= 7.2 Hz, $H_{Ar}$), 7.53 (*td*, 1 H, $^3J_{HH}$= 8.8, $^4J_{HH}$: 1.6 Hz, $H_{Ar}$), 7.77 (*dd*, 1 H, $^3J_{HH}$= 7.2, $^4J_{HH}$: 1.6 Hz, $H_{Ar}$), 13.66 (*s*, 1 H, OH). **$^{13}$C NMR** (100 MHz, DMSO-d6) δ: 21.4 ($CH_3$), 48.6, 56.4 ($CH_2$), 112.3, 119.0 (C = C), 127.6, 130.2, 133.1, 136.4, 138.4 (C = $C_{Ar}$), 144.1, 145.2 ($CO_2$), 165.0 (C = N).

*Prepration and characterization of 3,3'-((2E,12E)-3,6,9,12-tetraazatetradeca-2,12-diene-2,13-diyl)bis(4-hydroxy-2 H-chromen-2-one) [3c]*

Using triethylenetetramine, this Schiff base (compound **3c**) was synthesized similarly to compound **3b**. Triethylenetetramine was injected into the solution of 3-acetyl-4-hydroxycoumarin (1:2 molar ratio) in absolute MeOH (10 mL) and refluxed at 65 °C for 6 h. Following the completion of the reaction the mixture was cooled to room temperature and filtered. The yellow residue was washed several times with cold MeOH until the filtrate became colorless and then the white powder solid residue was vacuum-dried (Yield = 0.352 g, 68%).

**m.p.**: 207–209 °C; **Elemental analysis** for $C_{28}H_{30}N_4O_6$: **Found**: C: 64.87, H: 5.86, N: 10.77; **Calculated**: C: 64.85, H: 5.83, N: 10.80; **IR** ($\upsilon_{max}$, $cm^{-1}$): (NH): 3334, (OH): 3253, ($C_{Ar}H$): 3055, ($C_{SP}{}^3$-H): 2900, (C = O): 1735, (C = N): 1665, (C = C): 1651, (C = $C_{Aryl}$): 1482. **Mass**, m/z (%): Molecular ion: 518.10 ($M.^+$, 15), base peak: 316.2 ($M.^+$-202, 100). **$^1$H NMR** (400 MHz, DMSO-d6) δH: 2.38 (*s*, 3H, $CH_3$), 2.53 (*brs*, 1 H, NH), 2.67 (*s*, 2 H, $CH_2$), 2.79 (*t*, 2 H, $^3J_{HH}$= 6.8 Hz, $CH_2$), 3.69 (*t*, 2 H, $^3J_{HH}$= 6.8 Hz, $CH_2$), 7.52 (t*d*, 1 H, $^3J_{HH}$= 8.4, $^4J_{HH}$: 1.2 Hz, $H_{Ar}$), 7.56 (*d*, 1 H, $^3J_{HH}$= 8.4 Hz, $H_{Ar}$), 7.93 (*td*, 1 H, $^3J_{HH}$= 8.8, $^4J_{HH}$: 1.6 Hz, $H_{Ar}$), 8.03 (*dd*, 1 H, $^3J_{HH}$= 8.0, $^4J_{HH}$: 1.6 Hz, $H_{Ar}$), 17.070 (*brs*, 1 H, OH). **$^{13}$C NMR** (100 MHz, DMSO-d6) δ: 25.1 ($CH_3$), 48.4, 49.5, 56.4 ($CH_2$), 95.5, 98.0 (4 C = C), 111.7,117.5, 125.4, 136.1, 160.7, and 161.8 (C = $C_{Ar}$), 154.2 ($CO_2$), 180.0 (C = N).

*Prepration and characterization of 1,3-bis((E)-1-(4-hydroxy-2-oxo-2 H-chromen-3-yl)ethylidene)urea [3d]*

Compound **3d** was synthesized from urea (1 mmol, 0.06 g) and 3-acetyl-4-hydroxycoumarin (2 mmol, 0.408 g). This mixture was refluxed in 10 mL of absolute MeOH for 4 h. To provide a white solid product, a Dean/Stark trap was used to remove water formed during the reaction. Following thorough filtering and washing with diethyl ether, the product was rinsed 2–3 times with cold MeOH and dried under vacuum (Yield = 0.33 g, 78%).

**m.p.**: 134–136 °C; **Elemental analysis** for $C_{23}H_{16}N_2O_7$: **Found**: C: 63.91, H: 3.75, N: 6.45; **Calculated**: C: 63.89, H: 3.73, N: 6.48; **IR** ($\upsilon_{max}$, $cm^{-1}$): (OH): 3420, ($C_{Ar}H$): 3099, 3055, ($C_{SP}{}^3$-H): 2950, (C = O): 1740, 1718, (C = N): 1688, (C = $C_{Aryl}$): 1489, 1427. **Mass**, m/z (%): Molecular ion: 432.10 ($M.^+$, 15), base peak: 230 ($M.^+$-202, 100). **$^1$H NMR** (400 MHz, DMSO-d6) δH: 2.63 (*s*, 3H, $CH_3$), 7.25 (*d*, 1 H, $^3J_{HH}$= 8.4 Hz, $H_{Ar}$), 7.29 (*td*, 1 H, $^3J_{HH}$= 8.4, $^4J_{HH}$: 1.2 Hz, $H_{Ar}$), 7.63 (*td*, 1 H, $^3J_{HH}$= 8.4, $^4J_{HH}$: 1.2 Hz, $H_{Ar}$), 7.94 (*dd*, 1 H, $^3J_{HH}$= 6.0, $^4J_{HH}$: 1.6 Hz, $H_{Ar}$), 12.05 (*s*, 1 H, OH). **$^{13}$C NMR** (100 MHz, DMSO-d6) δ: 23.9 ($CH_3$), 101.0, 133.8 (C = C), 116.50, 116.52, 154.6, 155.7, 159.5, 161.9 (C = $C_{Ar}$), 163.9 ($CO_2$), 178.3 (C = N), 181.0 (C = O).

*Prepration and characterization of 1,3-bis((E)-1-(4-hydroxy-2-oxo-2 H-chromen-3-yl)ethylidene)guanidine [3e]*

A methanolic mixture (15 mL) of 3-acetyl 4-hydroxycoumarin (2 mmol, 0.408 g) with guanidine hydrochloride (1.0 mmol, 0.1 g). This mixture was refluxed in 10 mL of absolute MeOH for 4 h. The solution was treated with a few drops of triethylamine to act as both a catalyst and a base. The mixture was stirred under reflux conditions for 6 h. Using a Dean/Stark trap, the water formed in the reaction was trapped, resulting in a white solid product. Cooling, filtering, and several washes with distilled water were performed on the mixture. Final purification took place by re-crystallization from EtOH and drying in a vacuum. (Yield = 0.32 g, 74%).

**m.p.**: 204 °C; **Elemental analysis** for $C_{23}H_{17}N_3O_6$: **Found**: C: 64.06, H: 3.99, N: 9.72; **Calculated**: C: 64.04, H: 3.97, N: 9.74; **IR** ($\upsilon_{max}$, $cm^{-1}$): (NH): 3334, (OH): 3258, ($C_{Ar}H$): 3109, ($C_{SP}{}^3$-H): 2924, 2868, (C = O): 1737, (C = N): 1680, 1656, (C = $C_{Aryl}$): 1464. **Mass**, m/z (%): Molecular ion: 431.10 ($M.^+$, 12.5), base peak: 229 ($M.^+$-202, 100). **$^1$H NMR** (400 MHz, DMSO-d6) δH: 2.68 (*s*, 3H, $CH_3$), 7.44 (*d*, 1 H, $^3J_{HH}$= 7.2 Hz, $H_{Ar}$), 7.45 (*t*, 1 H, $^3J_{HH}$= 7.2 Hz, $H_{Ar}$), 7.84 (*td*, 1 H, $^3J_{HH}$= 7.6, $^4J_{HH}$: 1.2 Hz, $H_{Ar}$), 8.03 (*d*, 1 H, $^3J_{HH}$= 6.8 Hz, $H_{Ar}$), 9.63 (*s*, 0.5 H, =NH), 17.73 (*s*, 1 H, OH). **$^{13}$C NMR** (100 MHz, DMSO-d6) δ: 24.2 ($CH_3$), 110.9, 112.0 (C = C), 115.30, 117.3, 125.2, 125.7, 137.1, 154.6 (C = $C_{Ar}$), 159.7 (C = NH), 173.7 ($CO_2$), 205.9 (C = N).

*Prepration and characterization of 1,3-bis((E)-1-(4-hydroxy-2-oxo-2 H-chromen-3-yl)ethylidene)thiourea [3f]*

The Schiff base **3f** was prepared from thiourea (0.076 g, 1 mmol) and 3-acetyl 4-hydroxycoumarin (0.408 g, 2 mmol) in 10 mL absolute MeOH. After refluxing for 2 h, the water produced as a result of the reaction was eliminated using a Dean/Stark system. Subsequently, the solution was allowed to cool down to ambient temperature and the solvent was separated through filtration. Using chloroform, the residue was thoroughly washed. Recrystallization of the solid complex was accomplished by mixing 1:2 (v/v) MeOH and petroleum ether/chloroform, followed by vacuum drying of the yellow precipitate. (Yield = 0.35 g, 79%).

**m.p.**: 200–202 °C; **Elemental analysis** for $C_{23}H_{16}N_2O_6S$: **Found**: C: 61.64, H: 3.58, N: 6.27; **Calculated**: C: 61.60, H: 3.60, N: 6.25; **IR** ($\upsilon_{max}$, $cm^{-1}$): (OH): 3420, ($C_{Ar}H$): 3053, ($C_{SP}{}^3$-H): 2950, (C = O): 1745, 1709, (C = N): 1643, (C = $C_{Aryl}$): 1401, (C = S): 1205. **Mass**, m/z (%): Molecular ion: 448.20 ($M.^+$, 10.4), base peak: 246.3 ($M.^+$-

202, 100). **$^{1}$H NMR** (400 MHz, DMSO-d6) δH: 2.68 (*s*, 3H, $CH_3$), 7.43–747 (*m*, 2 H, $H_{Ar}$), 7.84 (*td*, 1 H, $^{3}J_{HH}$= 6.0, $^{4}J_{HH}$: 1.6 Hz, $H_{Ar}$), 8.04 (*dd*, 1 H, $^{3}J_{HH}$= 6.8, $^{4}J_{HH}$: 1.6 Hz, $H_{Ar}$), 17.63 (*brs*, 1 H, OH). **$^{13}$C NMR** (100 MHz, DMSO-d6) δ: 23.8 ($CH_3$), 102.0, 137.3 (C = C), 125.2, 125.7, 137.5, 138.0, 154.6, 155.7 (C = $C_{Ar}$), 173.7 ($CO_2$), 178.3 (C = N), 188.2 (C = S).

*Prepration and characterization of (E)-N-((E)-1-(4-hydroxy-2-oxo-2 H-chromen-3-yl)ethylidene)-2-(1-(4-hydroxy-2-oxo-2 H-chromen-3-yl)ethylidene)hydrazine-1carboxamide [3 g]*

The Schiff base **3 g** was prepared by reacting 0.075 g (1 mmol) semicarbazide and 0.408 g 3-acetyl-4-hydroxycoumarin (2 mmol) in 10 mL absolute MeOH taken into a round-bottomed flask and then the mixture was heated at 65 °C for about 4 h. After reaction completion, the mixture was filtered and washed with cold EtOH. The creamy product was obtained and dried at 60 °C overnight. (Yield = 0.36 g, 82%).

**m.p.**: 205–208 °C; **Elemental analysis** for $C_{23}H_{17}N_3O_7$: **Found**: C: 61.71, H: 3.79, N: 9.42; **Calculated**: C: 61.75, H: 3.83, N: 9.39; **IR** ($\upsilon_{max}$, $cm^{-1}$): (NH): 3425, ($C_{Ar}$H): 3055, ($C_{SP}{}^{3}$-H): 2867, (C = O): 1728, 1670, (C = N): 1646, (C = $C_{Aryl}$): 1599. **Mass**, m/z (%): Molecular ion: 447.10 ($M.^{+}$, 18.1), base peak: 245.0 ($M.^{+}$-202, 100). **$^{1}$H NMR** (400 MHz, DMSO-d6) δH: 2.63 (*s*, 3H, $CH_3$), 7.24 (*dd*, 1 H, $^{3}J_{HH}$= 7.6, $^{4}J_{HH}$: 0.8 Hz, $H_{Ar}$), 7.28 (*td*, 1 H, $^{3}J_{HH}$= 7.2, $^{4}J_{HH}$: 0.8 Hz, $H_{Ar}$), 7.60 (*td*, 1 H, $^{3}J_{HH}$= 9.2, $^{4}J_{HH}$: 1.6 Hz, $H_{Ar}$), 7.94 (*dd*, 1 H, $^{3}J_{HH}$= 6.4, $^{4}J_{HH}$: 1.6 Hz, $H_{Ar}$), 9.35 (*s*, 0.5 H, NH), 15.20 (*s*, 1 H, OH). **$^{13}$C NMR** (100 MHz, DMSO-d6) δ: 16.5 ($CH_3$), 94.0, 101.0 (C = C), 116.5, 120.6, 123.9, 125.7, 133.7, 153.3 (C = $C_{Ar}$), 162.1 ($CO_2$), 166.3 (C = N), 178.2 (N-C = O).

*Prepration and characterization of 3,3'-((1E,1'E)-(cyclohexane-1,2-diylbis(azanylylidene))bis(ethan-1-yl-1-ylidene))bis(4-hydroxy-2 H-chromen-2-one) [3 h]*

The Schiff base **3 h** was prepared by adding 3-acetyl-4-hydroxycoumarin (0.408 g, 2 mmol) in 10 mL absolute MeOH. When the solid was completely dissolved, (1R,2R)-(-)-1,2-diaminocyclohexane (0.114 g, 1 mmol) was added to the solution and refluxed for 12 h. The reaction mixture was then cooled to room temperature, and filtered to give a white solid, which was washed with cold MeOH. Then, the precipitate was dried under a vacuum (0.34 g, 71%).

**m.p.**: 263 °C; **Elemental analysis** for $C_{28}H_{26}N_2O_6$: **Found**: C: 69.16, H: 5.43, N: 5.79; **Calculated**: C: 69.12, H: 5.39, N: 5.76; **IR** ($\upsilon_{max}$, $cm^{-1}$): (OH): 3302, ($C_{Ar}$H): 3115, 3042 ($C_{SP}{}^{3}$-H): 2962, 2925, (C = O): 1734, (C = N): 1682, (C = $C_{Aryl}$): 1534. **Mass analysis**, m/z Molecular ion: 486.30 ($M.^{+}$, 21.42), base peak: 284.1 ($M.^{+}$-202, 100). **$^{1}$H NMR** (400 MHz, DMSO-d6) δH: 1.55–1.74 (*m*, 4 H, $CH_2$), 2.50 (*s*, 3H, $CH_3$), 3.72 (*d*, 1 H, $^{3}J_{HH}$= 6.0 Hz, CH), 7.20 (*d*, 1 H, $^{3}J_{HH}$= 8.0 Hz, $H_{Ar}$), 7.27 (*t*, 1 H, $^{3}J_{HH}$= 7.6 Hz, $H_{Ar}$), 7.60 (*t*, 1 H, $^{3}J_{HH}$= 7.2 Hz, $H_{Ar}$), 7.89 (*d*, 1 H, $^{3}J_{HH}$= 8.0 Hz, $H_{Ar}$), 14.26 (brs, 1 H, OH). **$^{13}$C NMR** (100 MHz, DMSO-d6) δ: 23.4 ($CH_3$), 97.4, 103.0 (C = C), 110.5, 116.8, 120.5 (C-N), 124.4, 126.0, 133.6, 134.8, 141.5, and 153.4 (C = $C_{Ar}$), 156.3 ($CO_2$), 181.6 (C = N).

*Prepration and characterization of 3,3'-((1E,1'E)-(pyridine-2,3-diylbis(azaneylylidene))bis(ethan-1-yl-1-ylidene))bis(4-hydroxynaphthalen-2(1 H)-one) [3i]*

To the solution of 2,3-diaminopyridine (0.109 g, 1 mmol) and 3-acetyl-4-hydroxycoumarin (0.408 g, 2mmol) in dried MeOH (10 mL), acetic acid was added. The reaction mixture was refluxed for about 12–14 h at 65 ℃ (TLC, methanol: hexane 1:4 ) and then cooled to room temperature. The separated white precipitate was recrystallized from hot EtOH and vacuum-dried for 1 h (Yield = 0.33 g, 68% ).

**m.p.**: 236–240 °C; **Elemental analysis** for $C_{29}H_{23}N_3O_6$: **Found**: C: 72.94, H: 4.93, N: 8.84; **Calculated**: C: 72.94, H: 4.96, N: 8.80; **IR** ($\upsilon_{max}$, $cm^{-1}$): (OH): 3423, ($C_{Ar}$H): 3079 ($C_{SP}{}^{3}$-H): 2855, 2781, (C = O): 1734, (C = N): 1655, (C = $C_{Aryl}$): 1508. **Mass analysis**, m/z (%): Molecular ion: 481.20 ($M.^{+}$, 6.6), base peak: 279.1 ($M.^{+}$-202, 100). **$^{1}$H NMR** (400 MHz, DMSO-d6) δH: 2.58 (*s*, 3H, $CH_3$), 7.21 (*t*, 1 H, $^{3}J_{HH}$= 7.6 Hz, $H_{Ar}$), 7.25 (*d*, 1 H, $^{3}J_{HH}$= 8.0 Hz, $H_{Ar}$), 7.60–7.71 (*m*, 2.5 H, $H_{Ar}$), 7.79 (*d*, 1 H, $^{3}J_{HH}$= 7.6 Hz, $H_{Ar}$), 15.41 (*s*, 1 H, OH). **$^{13}$C NMR** (100 MHz, DMSO-d6) δ: 20.5 ($CH_3$), 24.4, 30.5 ($CH_2$), 65.1.5 (C-N), 98.3, 110.9 (C = C), 116.1, 120.0, 133.7, 134.1, 164.1, 164.9 (C = $C_{Ar}$), 153.4 ($CO_2$), 180.0 (C = N).

*Prepration and characterization of 3,3'-((1E,1'E)-((6-amino-1,3,5-triazine-2,4-diyl)bis(azanylylidene))bis(ethan-1-yl-1-ylidene))bis(4-hydroxy-2 H-chromen-2-one) [3j*

The Schiff base **3j** was synthesized by dissolving 3-acetyl 4-hydroxycoumarin (0.408 g, 2 mmol) and melamine (0.126 g, 1.0 mmol) in 10 mL of absolute MeOH and three drops of acetic acid. The reaction mixture was heated under reflux at 65 °C for 10–12 h (TLC, methanol: hexane 3:7 ). Once the reaction was completed, the resulting product underwent filtration, followed by treatment with DI water, and then drying at r.t. This process led to the formation of a solid substance with a dark green color (Yield = 0.38 g, 76%).

**m.p.**: 238–240 °C; **Elemental analysis** for $C_{25}H_{18}N_6O_6$: **Found**: **C**: 60.28, **H**: 3.67, **N**: 16.89; **Calculated: C**: 60.24, **H**: 3.64, **N**: 16.86; **IR** ($\upsilon_{max}$, $cm^{-1}$): (OH): 3425, (NH): 3328, 3270, ($C_{Ar}$H): 3100 ($C_{SP}{}^{3}$-H): 2858, 2786, (C = O): 1746, (C = N): 1654, (C = $C_{Aryl}$): 1511, 1486. **Mass**, m/z (%): Molecular ion: 498.2 ($M.^{+}$, 7.3) base peak: 206.1 ($M.^{+}$-202, 100). **$^{1}$H NMR** (400 MHz, DMSO-d6) δH: 2.60 (*s*, 3H, $CH_3$), 6.58 (*s*, 1 H, $NH_2$), 7.32 (*d*, 1 H, $^{3}J_{HH}$= 7.6 Hz, $H_{Ar}$), 7.35 (*d*, 1 H, $^{3}J_{HH}$= 7.2 Hz, $H_{Ar}$), 7.67 (*td*, 1 H, $^{3}J_{HH}$= 6.4, $^{4}J_{HH}$= 1.6 Hz, $H_{Ar}$), 7.99 (*dd*, 1 H, $^{3}J_{HH}$= 4.8 Hz, $^{4}J_{HH}$= 1.6 Hz, $H_{Ar}$), 15.34 (*brs*, 1 H, OH). **$^{13}$C NMR** (100 MHz, DMSO-d6) δ: 21.1 ($CH_3$), 57.7, 64.6 (C-N), 98.2, 110.0 (C = C), 116.8, 124.3, 126.1, 128.4, 129.7, 132.6 (C = $C_{Ar}$), 153.6 ($CO_2$), 161.2, 162.3, 177.0 (C = $C_{pyridin}$), 188.5 (C = N).

A complete list of spectral data for all synthesized compounds 2 and 3a–j is available in the supplementary material.

## Microbial susceptibility test

Antimicrobial analysis was conducted following the National Committee for Clinical Laboratory Standards method[39]. Compounds 3a-j were tested for their minimum inhibitory concentration (MIC) against *E. coli*,

*Staphylococcus aureus*, *Pseudomonas aeruginosa*, and *Bacillus subtilis* following the Clinical and Laboratory Standards Institute (CLSI) guidelines[40]. Each compound was prepared in concentrations ranging from 0.002 to 5 mM in DMSO (100 µL) and then added to 96-well plates. The bacterial turbidity was adjusted using a half McFarland standard in a freshly cultured suspension in normal saline. This suspension was diluted 1:100 in Müller Hinton Broth, and 100 µL were introduced into each well, resulting in a bacterial concentration of $0.5–1 \times 10^6$ CFU/mL. The concentration in each well was then reduced by half (0.001–2.5 mM) to achieve the final concentration. The plates were incubated at 37 °C for 22 h, after which the MIC was determined. Standard antibiotics Metronidazole and Sulfadiazine were used as controls, and all MIC assays were performed in triplicate, with the average values reported.

## Antioxidant test

The DPPH method[41] was used to investigate the antioxidant activity of compounds **2** and **3a-j**. A spectrophotometric method was employed to measure antioxidant behavior at each concentration. Generally, a sample solution (1 mg/mL) in MeOH was provided. After adding 1 mL of this solution to a test tube including 1 mL of DPPH radical in methanol (0.1 mM), the solution was shaken vigorously in the dark condition for 60 min. The measurements were taken at 517 nm to evaluate the absorbance of DPPH, which was applied to calculate the percentage of scavenging capability for each concentration. The inhibition percentage was calculated using the following formula. The reported values are the mean values of three repetitions of each experiment:

$$\% \text{ Inhibition} = (\text{Ac - As})/\text{Ac x } 100$$

The absorbance of compounds (Fig. 1) (2 and 3a-j) and the ascorbic acid (AA) as control were measured at 517 nm and compared to determine the antioxidant potential of the synthesized compounds (Fig. 1). Positive control (AA) was employed to verify the results' accuracy. Based on an identical Aa batch, antioxidant potency was measured at 82.3%. After three repeats, the values were presented as an average ± standard deviation (SD).

## Antifungal test

The experiment employed four prevalent fungal strains, namely *Aspergillus glaucus*, *Aspergillus niger*, *Candida albicans*, and *Penicillium verrucosum*. These strains were obtained from the biochemistry Laboratory, Department of Biology, School of Science, University of Mazandaran.

To assess antifungal susceptibility, the procedures outlined in the CLSI document M27-A2[42] were followed. Ketoconazole stock solutions were produced using water. The dilutions that followed were carried out in RPMI 1640 medium, which had a pH of 7.0 and was adjusted using 0.165 M morpholino propane sulfonic acid buffer.

In microdilution trays, each well was filled with 100 µL of serially diluted compounds or the standard antifungal drug, ketoconazole (concentration range: 0.244 to 500 µg/mL). Following this, 100 µL of the diluted fungal inoculum was added to achieve a final volume of 200 µL per well, with an inoculum size of 103 CFU/mL. We added control wells for growth (without drug) and sterility.

Subsequently, the trays were placed in an incubator set at 35 °C in ambient air. After 48 h of incubation, the minimum inhibitory concentrations (MICs) were visually determined as the lowest concentration of the

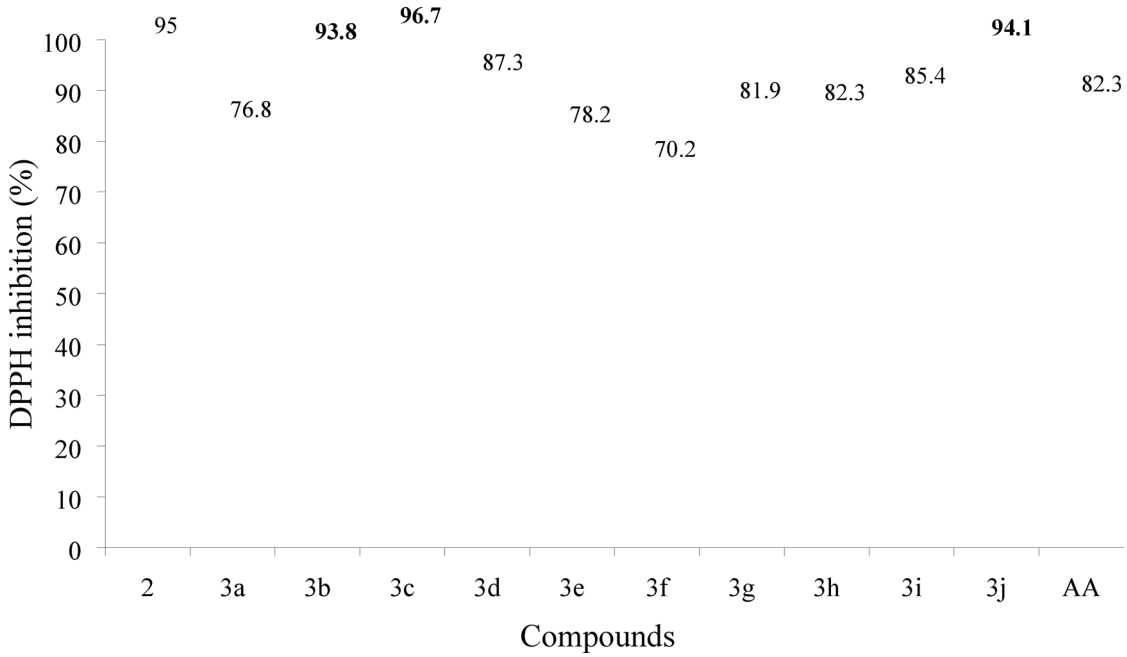



**Fig. 1**. Antioxidant activity of the prepared compounds 2, and 3a-j.

compound that inhibited visible fungal growth. The MIC values for the tested compounds and the standard drug were determined as the average of three independent measurements.

### Cytotoxicity evaluation

The cytotoxic effects of compounds 3a through 3j were assessed using the MTT method[43] against the *MCF-7* (human breast cancer cell line), *A549* (adenocarcinoma human alveolar basal epithelial cells), and a normal cell line, *BEAS-2B* (human normal bronchial epithelium cell line). Initially, cells were seeded at a density of $1 \times 10^4$ per well in 96-well plates and allowed to adhere overnight. Subsequently, various concentrations of compounds **3a** through **3j**, along with the reference drug doxorubicin (concentrations of 31, 62, 125, 250, and 500 µg/mL), were introduced into the wells. These solutions were incubated for 48 h to allow for the assessment of cellular toxicity. The medium was then supplemented with a 5 mg/mL MTT solution in PBS, which was incubated at 37 °C for an additional 4 hours to induce formazan crystallization. This process was followed by the dissolution of the formazan crystals in 100 µL DMSO, facilitating the measurement of absorbance at 570–690 nm using a plate reader, thereby quantifying the cellular viability.

### Statistical data analysis

The $IC_{50}$ values of compounds 3a-j were established through a systematic process. All compounds were evaluated at various concentrations in cell-based assays, and all experiments were carried out in triplicate to ascertain reliability. The data was analyzed using GraphPad Prism 9 software, and data was presented as mean values with standard deviation. Statistical significance was determined using two-way ANOVA analysis followed by Tukey's multiple comparison test, where differences were deemed to be significant at $p < 0.05$[44].

### Molecular docking study

An investigation was carried out using the MOE software version 2022.02 to examine the interactions between compounds **3b**, **3c**, and **3j** with the *FGFR1* and *cIAP1-BIR3* proteins. The crystallographic structures of these proteins, obtained from the Protein Data Bank (PDB) (www.rcsb.org), were identified by PDB IDs 3GQL[45] and 4KMN[46]. The proteins were prepared for modeling by removing the standard ligand molecule from the active site, fixing the heavy atoms, and adding hydrogen atoms to the protein structure. The root mean square (RMS) gradient was adjusted to 0.01 kcal/mole, the RMS distance was set to 0.1 Å, and the partial charges were computed using the MMFF94x force field. The final step involved saving the ligand interaction structure as a PDB file, which was then visualized using the BIOVIA Discovery Studio 2024 v24.1.0.334. The chemicals were found to accurately align with the active sites of the proteins in both 2D and 3D representations.

*Ligand preparation and validation*

Ligands were generated via MOE's LigX module at pH 7.4 with protonation for docking and energy minimization using MMFF94x. Validation of docking protocols was performed by re-docking the co-crystallized ligands from the corresponding PDB structures (3GQL for *FGFR1* and 4KMN for *cIAP1-BIR3*). The RMSD cutoff of 2.0 Å was observed confirming docking accuracy.

## Results and discussion

### Chemistry

Scheme 1 demonstrates the preparation of 3-acetyl-4-hydroxycoumarin-derived Schiff bases. The reaction of 3-acetyl-4-hydroxycoumarin (**2**) and diethylenetriamine was selected as a model reaction (Compound **3b**).

A variety of solvents were utilized in this study, including MeOH, $CH_3CN$, MeOH, THF, and EtOH. The reaction was conducted at room and reflux temperatures in each solvent. Based on the conditions shown in Table 1, the reaction in MeOH under reflux conditions produced the best yield (95%) (**entry 8**). It was chosen due to its optimal reaction conditions. Methanol is a polar solvent with a high dielectric constant, which enables it to effectively dissolve a wide range of organic compounds, including both 3-acetyl-4-hydroxycoumarin and diethylenetriamine. The ability of methanol to dissolve reactants is crucial for promoting their interaction and facilitating the formation of the desired product. Additionally, methanol's polarity may enhance the solubility of reaction intermediates and promote their conversion to the final Schiff base product. In addition, methanol is relatively stable under reflux conditions, making it suitable for prolonged heating without significant

| Entry | Solvents | Temperature [a] °C | Time (h) | Yields [b] (%) |
|---|---|---|---|---|
| 1 | EtOH | 25 | 6 | 20 |
| 2 | THF | 25 | 7 | 25 |
| 3 | $CH_3CN$ | 25 | 7 | 33 |
| 4 | MeOH | 25 | 7 | 65 |
| 5 | EtOH | 75 | 2 | 80 |
| 6 | THF | 66 | 4 | 50 |
| 7 | $CH_3CN$ | 82 | 4 | 67 |
| 8[c] | MeOH | 65 | 1 | 95 |

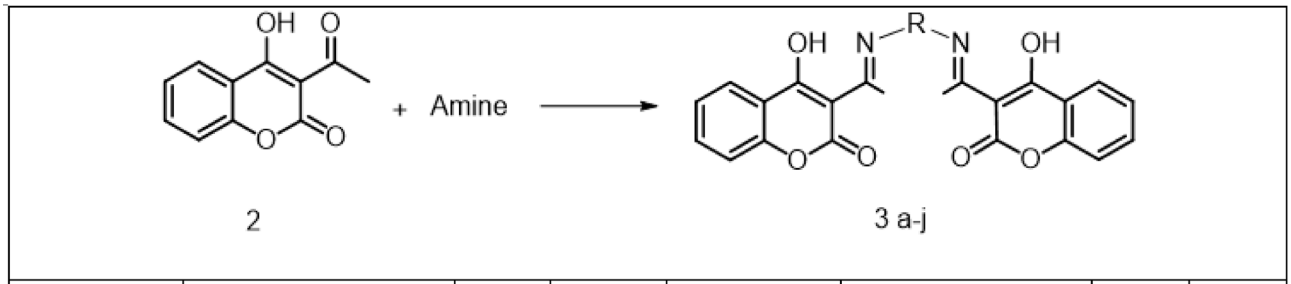
**Table 1**. Optimum conditions for standard reaction. [a] Reaction conditions: 3-acetyl-4-hydroxycoumarin (2 mmol), diethylenetriamine (1 mmol), and solvent (10 mL). [b] Isolated yield. [c]

decomposition or side reactions. In contrast, ethanol showed lower efficiency under similar conditions, likely due to slightly weaker solvation and slower reaction kinetics.

Using optimal reaction conditions, other diamines were reacted with 3-acetyl-4-hydroxycumarin to form products 3a–j with excellent yields (Table 2). Using $^{1}$H NMR, $^{13}$C NMR, IR, CHN, and mass spectra, the structures of compounds **3a-j** have been determined. A complete list of spectral information for compounds **2** and **3a–j** is available in the supplementary material (Figs. S1-S11).

The $^{1}$H NMR spectrum of compound 3b in DMSO-d6 demonstrates 9 main peaks because of its symmetrical structure. A broad signal at 1.59 ppm for NH, a singlet at 2.64 ppm for $CH_3$ protons of the acetyl group, a triplet at 2.91 ppm for $CH_2$, another triplet at 3.66 ppm for $CH_2$, a doublet at 7.10 ppm, a triplet at 7.14 ppm, a triplet of doublet at 7.53 ppm, and a doublet of doublet at 7.77 ppm for ortho-disubstituted aromatic protons, and a broad signal at 13.66 ppm for the hydroxyl group (Fig. S3). It is observed that the proton-decoupled $^{13}$C NMR spectrum of the compound **3b** contains 13 signals consistent with the structure outlined (Fig. S3.2).

The mass spectrum of synthesized compound **3b** (Fig. S3.4) reveals the molecular ion peak ($M^{+\bullet}$) at m/z = 475 (8.3%) and a signal at m/z = 314 (15%) (for ($M^{+\bullet}$–[$C_9H_5O_3$]), also the base peak at m/z = 273 (100%) for ($M^{+\bullet}$-




2 3 a-j

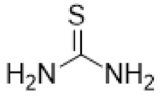
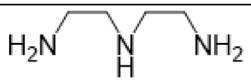
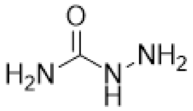
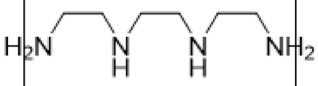
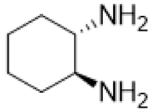
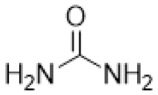
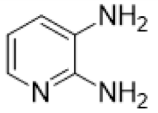
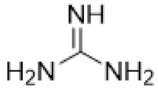
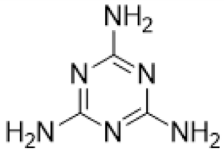
| Compound | Amine | Time (h) | Yield (%) [b] | Compound | Amine | Time (h) | Yield (%) |
|---|---|---|---|---|---|---|---|
| **3a** | $NH_2$-$NH_2$ | 1 | 85 | **3f** |  | 2 | 79 |
| **3b** |  | 1 | 95 | **3g** |  | 4 | 82 |
| **3c** |  | 6 | 68 | **3h** |  | 12 | 71 |
| **3d** |  | 4 | 78 | **3i** |  | 13 | 68 |
| **3e** |  | 4 | 74 | **3j** |  | 11 | 76 |

**Table 2**. Preparation of Coumarin-derived Schiff bases[a].
[a] Reaction condition: 3-acetyl-4-hydroxycoumarin (2) (2 mmol), amine (1 mmol), and MeOH (10 mL). [b] Isolated yield.

$[C_{11}H_8NO_3]$), a signal at m/z = 216 (7%) (for ($M^{+\bullet}$–[ $C_{14}H_{15}N_2O_3$]), which confirms the proposed symmetrical structure. Some fragmentations of compounds **3a** and **3b** are provided in Scheme S1 and S2.

Additionally, the mass spectrum of compound **3a** exhibits distinct peaks, which serve as evidence of its symmetrical structure (refer to Fig. S2.4). The spectrum reveals several key peaks that are crucial for differentiating between the intended symmetrical structure of compound **3a** and any potential monomer byproducts. Specifically, the following peaks are noteworthy:

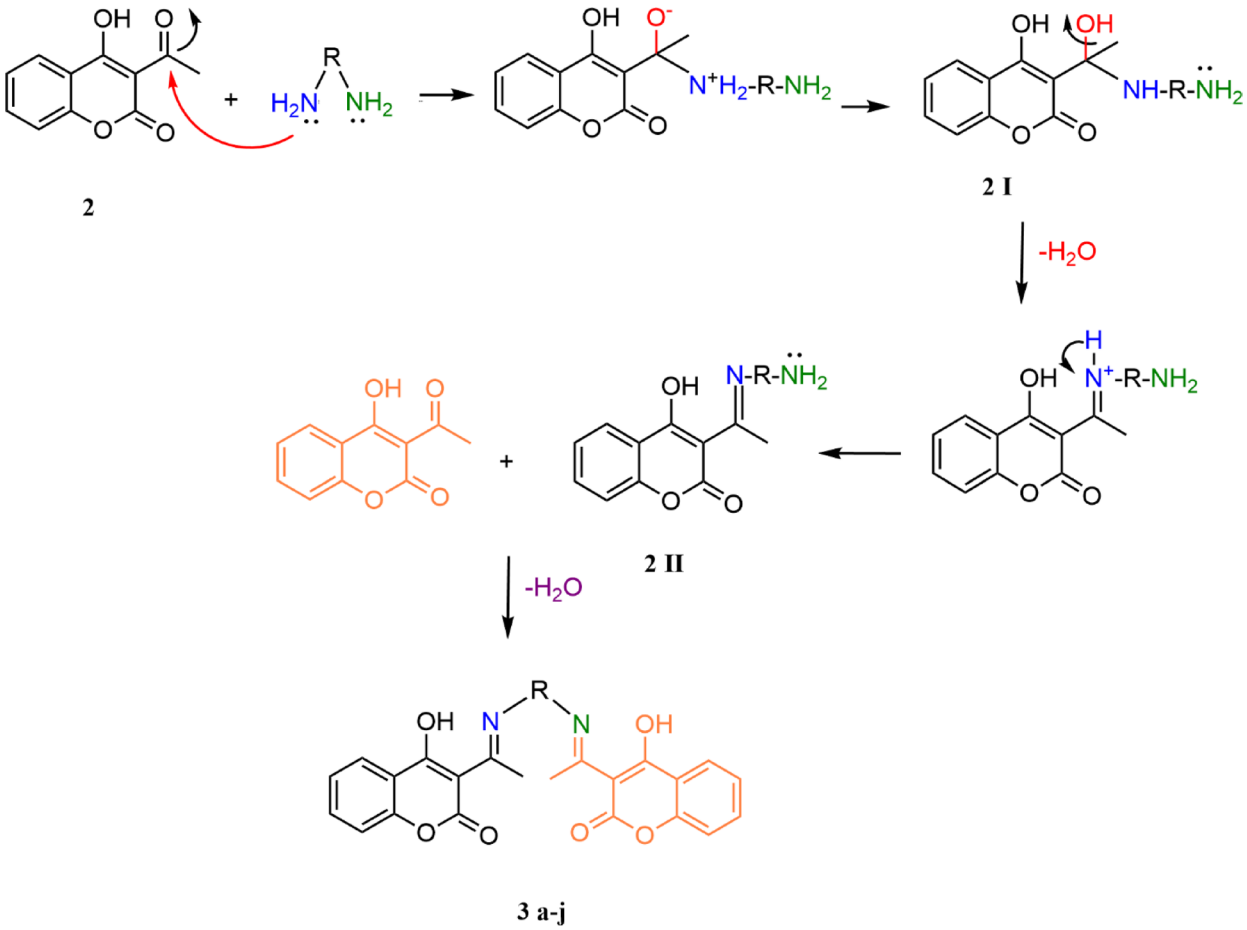
A molecular ion peak at m/z = 404 (7.1%), corresponding to ($M^{+\bullet}$). A signal at m/z = 389 (20%), indicative of ($M^{+\bullet}$–[Me]). A peak at m/z = 243 (7%), representing ($M^{+\bullet}$-[$C_9H_5O_3$]). Another peak at m/z = 226 (20%), corresponding to ($M^{+\bullet}$–[$C_9H_5O_3$ + OH]). A base peak at m/z = 202 (100%), which corresponds to ($M^{+\bullet}$–[$C_{11}H_8NO_3$]). A signal at m/z = 161 (30%), representing ($M^{+\bullet}$–[$C_{13}H_{11}N_2O_3$]). Lastly, a peak at m/z = 92 (30%), corresponding to ($M^{+\bullet}$–[$C_{11}H_8NO_3$ + $C_5H_4NO_2$]). These fragmentation patterns support the identification of the desired **3a** product.

Scheme 2 suggests a plausible mechanism based on data from the literature. The commercially available 4-hydroxycoumarin can be readily acetylated using acetyl chloride[47] or by reacting with acetic acid and $POCl_3$[15] to yield the starting reagent 3-acetyl-4-hydroxycoumarin (**2**). Based on the mechanism, the nucleophilic attack of an amino group of the diamine on the carbonyl group of compound **2** generates the hemiaminal intermediate (**2 I**), also known as carbinolamine. The intermediate (**2 I**) goes through a dehydration reaction to lose a water molecule, creating the Schiff base (**2 II**). Similarly, the amino group from the other side of the diamine then nucleophilically attacks the carbonyl group of compound **2** to generate the symmetric bisimine (**3**).

## Biological activity

*Antimicrobial evaluation*

The prepared Schiff bases (Compounds **3a-j**) were screened for antibacterial and antioxidant properties. The antibacterial efficacy of the synthesized compounds was evaluated using the MIC method, targeting both Gram-positive bacteria (Bacillus subtilis and Staphylococcus aureus) and Gram-negative bacteria (Pseudomonas aeruginosa and Escherichia coli). Metronidazole and Sulfadiazine, known antibacterial agents, were employed as reference standards to provide a more structurally and mechanistically relevant comparison with the synthesized compounds. These standards were selected due to their structural and mechanistic relevance, providing a more appropriate benchmark for assessing the antibacterial potency of the synthesized compounds.




**Scheme 2**. Suggested mechanism for synthesizing bisimines 3a-j.

As can be seen in Table 3 almost all the compounds (Compounds **3a-j**) are efficient against Gram-positive and negative bacteria except compound **3f**. The presence of thiourea groups in compound **3f** could prevent exhibiting antibacterial properties. Furthermore, the phenyl rings found in compounds **3i** and **3j** reduced their antibacterial properties. Despite these decreases, substituting a hydrogen atom in the R position (Compound **3a**) led to increased antibacterial efficacy. Based on comparisons with other derivatives, substance **3a** exhibits the highest antibacterial activity against *Staphylococcus aureus*. The results reported in Table 3 reveal that the tested compounds have greater antibacterial properties against Gram positive bacteria.

*Antioxidant evaluation*

DPPH (2,2-diphenyl-1-picrylhydrazyl) is inhibited by non-bonded electron pairs or exchangeable hydrogens in substituent groups within a structure[48]. Inhibiting DPPH radicals is generally performed using compounds containing substituent groups with lone pair electrons or exchangeable hydrogens. Based on the results of this study, compounds **3a-j** are highly effective at eliminating DPPH, as shown in Fig. 1. Among the synthesized compounds, compound **3c** exhibited the highest antioxidant activity (96.7%), even more than ascorbic acid's antioxidant activity on a standard basis. It appears that their antioxidant activity is affected by triethylenetetramine and diethylenetriamine substitutions. There may be a reason for this by the existence of more nitrogen atoms (N) as a polarized substitution, more non-bonding electrons, and more exchangeable protons in compounds **3b**, **3c**, and **3j**[49,50].

*Antifungal activity*

The antifungal potential of synthesized bisimine derivatives (Compounds **3a-j**) was evaluated against four clinically relevant fungal strains: *Aspergillus glaucus*, *Aspergillus niger*, *Candida albicans*, and *Penicillium verrucosum*. Using a standardized microdilution method with ketoconazole as positive control, we observed striking variations in antifungal efficacy across the compound series, as tabulated in Table 4.

Notably, the thiourea-containing derivative **3f** demonstrated exceptional broad-spectrum activity, with MIC values ranging from 1.95 to 31.25 µg/mL against all tested strains. This represents a 4–16 fold improvement over the parent compound **2** (MIC > 62.5 µg/mL). The thionyl group's potential to disrupt fungal membrane integrity may contribute to this enhanced activity, though the exact mechanism requires further investigation.

Other derivatives showed more selective inhibition patterns. Amino-substituted compounds (**3b**, **3j**) exhibited moderate activity (MIC 7.81–31.25 µg/mL), particularly against *C. albicans*. The triethylenetetramine analog **3c** showed intermediate potency (MIC 15.62–125 µg/mL). Simple hydrazine derivative **3a** displayed limited efficacy (MIC 31.25–125 µg/mL).

Interestingly, *C. albicans* emerged as the most susceptible strain, with all active compounds (**3b-j**) showing MIC values ≤ 31.25 µg/mL. This may reflect enhanced cell wall permeability or target accessibility in yeast versus filamentous fungi. The differential activity patterns across structural analogs suggest that both electronic properties (e.g., amino vs. thionyl substituents) and molecular geometry influence antifungal specificity.

Amino groups can act as nucleophiles, participating in nucleophilic aromatic substitution reactions that could potentially disrupt the fungal cell membrane (compounds **3b**, **3c**, **3 h**, and **3j**). Conversely, thionyl groups could potentially function as oxidizing agents, which might also impact the fungal cell (compound **3f**)[51].

*Cytotoxic activity*

The cytotoxic potential of synthesized compounds (**3a-j**) was evaluated against *MCF-7* breast cancer cells, *A549* lung adenocarcinoma cells, and normal *BEAS-2B* bronchial epithelial cells using the MTT viability assay. Doxorubicin served as the positive control, while compound **2** was included to establish baseline activity. Results

| Compounds [a] | Minimum Inhibitory Concentration (MIC) | | | |
|---|---|---|---|---|
| | Gram-negative bacteria | | Gram-positive bacteria | |
| | *Escherichia coli* | *Pseudomonas aeruginosa* | *Staphylococcus aureus* | *Bacillus subtilis* |
| 2 | 8.0 ± 1.4 | 7.0 ± 5.18 | 7.5 ± 0.7 | 7.0 ± 5.10 |
| a3 | 8.5 ± 0.7 | NE [b] | 5.10 ± 0.7 | 0.51 ± 20.3 |
| 3b | 4.1 ± 0.13 | 4.1 ± 0.11 | 7.0 ± 5.9 | 7.0 ± 5.10 |
| 3c | 22.3 ± 1.2 | 16.5 ± 0.7 | 8.0 ± 1.4 | 8.5 ± 0.7 |
| 3d | NE | 14.5 ± 0.7 | 15.0 ± 1.4 | 16.5 ± 0.7 |
| 3e | 11.5 ± 0.7 | 14.0 ± 1.4 | 4.1 ± 0.11 | 10.0 ± 1.4 |
| 3f | NE | NE | NE | NE |
| 3 g | 9.0 ± 1.4 | NE | 8.5 ± 0.7 | 18.5 ± 0.7 |
| 3 h | 20.3 ± 1.5 | 26.0 ± 1.7 | 18.5 ± 0.7 | NE |
| 3i | 4.1 ± 5.22 | 26.0 ± 1.7 | 12.5 ± 0.7 | 9.0 ± 1.4 |
| 3j | 18.5 ± 0.7 | 20.7 ± 15 | 13.0 ± 1.4 | 9.5 ± 0.7 |
| Metronidazole | 1.1 ± 6.19 | 5.0 ± 6.15 | 16.5 ± 0.7 | 7.1 ± 0.26 |
| Sulfadiazine | 5.1 ± 7.20 | 64.5 ± 0.26 | 21.7 ± 0.6 | 18.5 ± 0.7 |

**Table 3**. Testing the antibacterial activity of compounds 2 and 3a-j [a] Compounds concentration: 20 µg/mL. [b] Not Effective.

| Compound | MIC (µg/mL) | | | |
|---|---|---|---|---|
| | Aspergillus glaucus | Aspergillus niger | Candida albicans | Penicillium verrucosum |
| 3a | 31.25 ± 0.02 | 125 ± 0.28 | 125 ± 0.28 | 62.5 ± 0.03 |
| 3b | 31.25 ± 0.02 | 62.5 ± 0.03 | 7.81 ± 0.05 | 125 ± 0.28 |
| 3c | 125 ± 0.28 | 31.25 ± 0.02 | 15.62 ± 0.04 | 31.25 ± 0.02 |
| 3d | 62.5 ± 0.03 | 125 ± 0.28 | 31.25 ± 0.02 | 62.5 ± 0.03 |
| 3e | 125 ± 0.28 | 62.5 ± 0.03 | 31.25 ± 0.02 | 125 ± 0.28 |
| 3f | 31.25 ± 0.02 | 3.9 ± 0.01 | 3.9 ± 0.01 | 1.95 ± 0.07 |
| 3 g | 125 ± 0.28 | 125 ± 0.28 | 31.25 ± 0.02 | 62.5 ± 0.03 |
| 3 h | 31.25 ± 0.02 | 15.62 ± 0.04 | 31.25 ± 0.02 | 62.5 ± 0.03 |
| 3i | 62.5 ± 0.03 | 31.25 ± 0.02 | 31.25 ± 0.02 | 125 ± 0.28 |
| 3j | 31.25 ± 0.02 | 31.25 ± 0.02 | 62.5 ± 0.03 | 7.81 ± 0.05 |
| K* | 7.8 | 7.8 | 1.95 | 3.9 |

**Table 4**. Antifungal activity of prepared bisimine derivatives (3a-j). K* Ketoconazole.

| Compound | $IC_{50}$ ± SD (µM) | | |
|---|---|---|---|
| | A549 | MCF-7 | BEAS-2B |
| 2 | 29.17 ± 0.55 | 32.53 ± 0.72 | 28.92 ± 0.45 |
| 3a | 39.53 ± 1.1 | 33.63 ± 1.06 | 29.63 ± 0.08 |
| 3b | 8.75 ± 0.33 | 11.04 ± 0.01 | 13.33 ± 0.68 |
| 3c | 6.66 ± 0.41 | 7.52 ± 0.70 | 4.11 ± 0.44 |
| 3d | 19.69 ± 0.06 | 14.55 ± 0.05 | 21.93 ± 0.10 |
| 3e | 65.99 ± 0.36 | 19.61 ± 0.08 | 44.54 ± 0.78 |
| 3f | 6.66 ± 0.01 | 7.59 ± 0.01 | 9.01 ± 0.02 |
| 3 g | 20.75 ± 0.94 | 12.62 ± 0.11 | 50.29 ± 0.40 |
| 3 h | 6.56 ± 0.39 | 66.42 ± 0.90 | 5.46 ± 0.61 |
| 3i | 16.47 ± 0.22 | 10.63 ± 0.90 | 10.53 ± 0.1 |
| 3j | 5.58 ± 0.2 | 6.68 ± 0.16 | 64.29 ± 1.2 |
| Doxorubicin | 5.95 | 8.87 | 4.08 |

**Table 5**. Anti cancer activity. Each experiment was conducted in triplicate, and the $IC_{50}$ values were presented as mean ± SD.

summarized in Table 5 demonstrate significant variations in potency, with $IC_{50}$ values spanning 4.1–65.0 µM across the series.

Selectivity Index (SI) calculations, defined as: SI= $\frac{IC50\ (Normal\ cells)}{IC50\ (Cancer\ cells)}$.

Selectivity Index revealed critical structure-activity relationships. While compound **2** showed negligible cytotoxicity (possibly due to poor membrane permeability), its modified derivatives exhibited markedly different profiles. Compound **3a** displayed weak activity ($IC_{50}$ > 30 µM), likely constrained by steric hindrance from its hydrazine linker. In contrast, derivatives **3c** ($IC_{50}$ = 6.66 ± 0.41 µM in *A549*) and **3f** ($IC_{50}$ = 6.66 ± 0.01 µM in *A549*) showed potent anticancer effects, though their comparable toxicity to normal cells (SI < 2) limits therapeutic potential. The melamine-containing analog **3j** emerged as the lead candidate, demonstrating: Superior potency ($IC_{50}$ = 5.58 ± 0.2 µM in *A549* and 6.68 ± 0.16 µM in *MCF-7*), Exceptional selectivity (SI > 9.6), and Broad-spectrum activity against both cancer types. This remarkable performance may originate from compound **3j**'s unique electronic properties, the electron-deficient melamine core potentially facilitates:

- ROS generation through mitochondrial disruption[52].
- Multipoint hydrogen bonding with cellular targets.
- Enhanced DNA intercalation via planar stacking.

Notably, the piperidine-containing derivative **3i** showed cell-type dependent activity (*MCF-7* $IC_{50}$ = 10.63 ± 0.90 µM vs. *A549* $IC_{50}$ = 16.47 ± 0.22 µM), suggesting tissue-specific uptake or target expression may influence efficacy. Its marginal selectivity (SI ≈ 1) indicates need for further optimization.

## Molecular ducking study

Inspired by the findings of this research, exploring the potential of synthesized bisimines for developing new anti-cancer medications appears promising. Compounds **3b**, **3c**, **3f** and **3j** exhibit notable cytotoxic effects against *MCF7* and *A549*, making them prime candidates for further molecular investigations for a comprehensive

structural comparison. Utilizing docking simulation, the interaction between the synthesized bisimines and *FGFR1* and Anti-apoptotic protein was analyzed.

Drawing from the insights provided in the sources, the investigation into 4-hydroxycoumarin and its derivatives reveals a promising interaction with tyrosine kinase receptors (RTK)[53]. These receptors are pivotal in numerous carcinomas, particularly in pancreatic carcinoma, characterized by an excessive expression of tyrosine kinase receptors and their ligands. Consequently, we embarked on molecular docking studies, focusing on proteins capable of inhibiting the proliferation of tyrosine kinase receptors.

**FGFR1** This protein is notably overexpressed in a variety of cancers, including pancreatic carcinoma. Such overexpression can foster uncontrolled cell growth and metastasis, underscoring *FGFR1* as a compelling target for cancer therapy. The Fibroblast Growth Factor Receptor 1 (*FGFR1*), identified by the PDB ID 3GQL, presents a potential avenue for inhibiting tyrosine kinase receptors. If our synthesized ligand successfully inhibits *FGFR1*'s normal activation process, it could serve as a tyrosine kinase inhibitor. This mechanism would involve the ligand binding to *FGFR1* in a manner that hinders the receptor's ability to dimerize or oligomerize, thereby obstructing the autophosphorylation of the tyrosine kinase domain (TKD)[46]. Selection of *FGFR1* as a target for molecular docking was based on its established role in the progression of various cancers, particularly due to its overexpression in certain tumor types like pancreatic carcinoma. Literatures suggest that 4-hydroxycoumarin derivatives, structurally related to our synthesized bisimines, show promising interactions with tyrosine kinase receptors, including *FGFR1*[53,57].

**Anti-apoptotic protein (AIP)** The protein known as Anti-apoptotic protein (*AIP*), specifically *cIAP1-BIR3* (recognized by the PDB ID 4KMN), is significantly elevated in the majority of tumor cells, thereby facilitating their survival. The ligand's binding to the *BIR3* domain of *cIAP1* may disrupt its anti-apoptotic activity and thereby promote apoptosis in tumor cells[55].

Table S1 and S2 represented interactions between selected ligands with receptors. Compound **3b** demonstrated robust binding to *FGFR1* (PDB: 3GQL) through multiple interaction modes (Fig. 2A). The coumarin scaffold formed two key hydrogen bonds: (i) a 3.99 Å H-acceptor interaction between the carbonyl oxygen and Lys514, and (ii) a 4.35 Å bond with Asn568. A third hydrogen bond (5.56 Å) connected the compound's nitrogen to Arg627. The binding interface was further stabilized by twelve hydrophobic contacts (π-H and π-alkyl) with Leu484, Ala564, Leu630, Ala512, and Val492/561, yielding a strong binding affinity (ΔG = -8.2 kcal/mol) and precise pose prediction (RMSD = 0.143 Å).

In the *cIAP1-BIR3* binding pocket (PDB: 4KMN; Fig. 2B), **3b** adopted a distinct interaction profile. Three hydrogen bonds anchored the compound: (i) esteric oxygen, Trp323 (5.25 Å), (2) hydroxyl, Cys309 (3.92 Å), and (iii) amine, Glu311 (5.05 Å). Hydrophobic stabilization was provided by π-alkyl, π-π T-shaped, and π-H

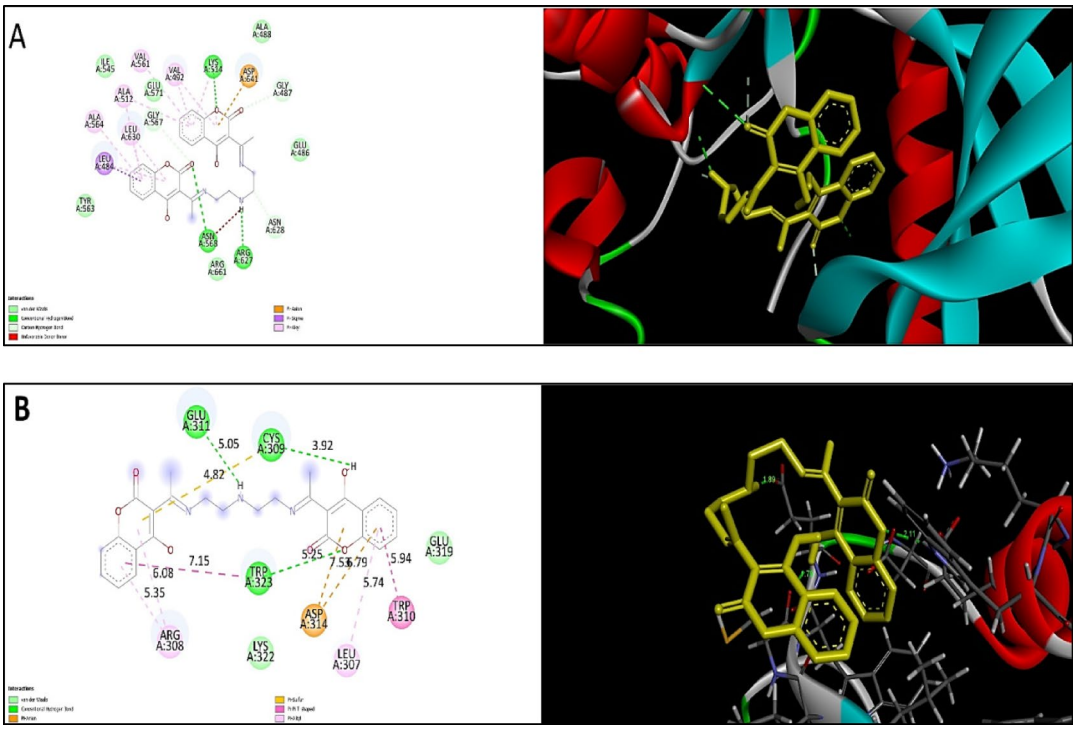



**Fig. 2**. 3D and 2D images of The binding model of compound 3b with (**A**) FGFR1 and (**B**) Anti-apoptotic protein (IAP). This figure was generated using the BIOVIA Discovery Studio 2024 v24.1.0.334.

interactions with Leu307, Arg308, Trp310, Trp323, and Asp314. The resulting binding energy (ΔG = -6.0 kcal/mol) and structural alignment (RMSD = 0.343 Å) confirm a stable, biologically relevant binding mode.

Our structural analysis reveals how compound **3c** engages with both *FGFR1* and *cIAP1-BIR3* through distinct yet complementary interaction networks. The binding profile with *FGFR1* (Fig. 3A) demonstrates an elegant balance of polar and hydrophobic contacts. The amine group reaches 5.35 Å across the binding pocket to donate a hydrogen bond to Glu571, while the esteric oxygen accepts one from Lys514 at 5.85 Å, distances that, while slightly longer than ideal, are compensated by an extensive hydrophobic network. Particularly noteworthy is the π-sulfur interaction with Met535 (3.9 Å), a relatively rare contact that may contribute to the compound's -7.7 kcal/mol binding affinity. The 0.991 Å RMSD suggests the pose is both stable and reproducible in simulations.

When binding *cIAP1-BIR3* (Fig. 3B), compound **3c** adopts a different strategy. The shorter hydrogen bond to Arg308 (4.39 Å) anchors the molecule, while the 5.74 Å interaction with Glu311 appears more dynamic. What really stabilizes this complex are the aromatic interactions, the compound nestles between Trp310 and Trp323 like a molecular sandwich, with π-π distances of 4.5–5.2 Å. The slightly higher RMSD (1.889 Å) hints at some flexibility in this binding mode, yet the −6.5 kcal/mol affinity remains pharmacologically relevant. This dual-target engagement profile, with its mix of conserved and unique interactions, helps explain compound **3c**'s promising cellular activity while suggesting opportunities for further optimization.

Figure 4A illustrates that Compound **3f** exhibits strong inhibitory properties, engaging in hydrophobic interactions and hydrogen bonding with the amino acid residues within the 3GQL binding site. The primary hydrogen bonds are observed between the C = O and esteric oxygen functional groups of the ligand and the Arg661, Asn568, and Lys514 amino acids of the enzyme, with bond lengths of 6.31, 4.53, and 5.73 Å, respectively. Additionally, this compound establishes van der Waals interactions with Lys514 and Gly487 through the -C = O and oxygen of the ester group. In the hydrophobic region, the coumarin ring is stabilized by Ile545, Met535, Asp641, and Ala640 residues. Another hydrophobic site is characterized by interactions between methyl groups and Val492 and Leu630 amino acids of the enzyme. These interactions collectively contribute to a binding score of -8.30 kcal/mol and an Rmsd value of 0.058, signifying a robust interaction between compound **3f** and the *FGFR1* receptor.

Furthermore, Compound **3f** demonstrates a variety of interactions, including two hydroxyl groups forming bonds with Glu306 and Arg308 (H-donor) with bond lengths of 2.40 Å and 2.44 Å, respectively. The coumarin rings also show binding with Trp310 through π–π interactions and with Arg308 and Glu319 through π-H interactions (Fig. 4B). These interactions exhibit a binding affinity of -7.20 kcal/mol and an Rmsd of 0.085.

Compound **3j** demonstrated potent inhibition of the tyrosine kinase receptor (3GQL) through an intricate network of molecular interactions (Fig. 5A). Table S1 and S2 represents that 11 distinct binding interactions, including two critical hydrogen bonds: (i) a 3.33 Å H-acceptor interaction between the ester carbonyl and Gly567, and (ii) a 3.34 Å H-donor interaction involving the hydroxyl group and Leu484 (Tables S1-S2). The binding pocket further stabilized **3j** through multiple hydrophobic contacts particularly noteworthy were the pi-alkyl interactions with Val492, Ala512, and Leu residues (484, 630), which likely shield the ligand from aqueous

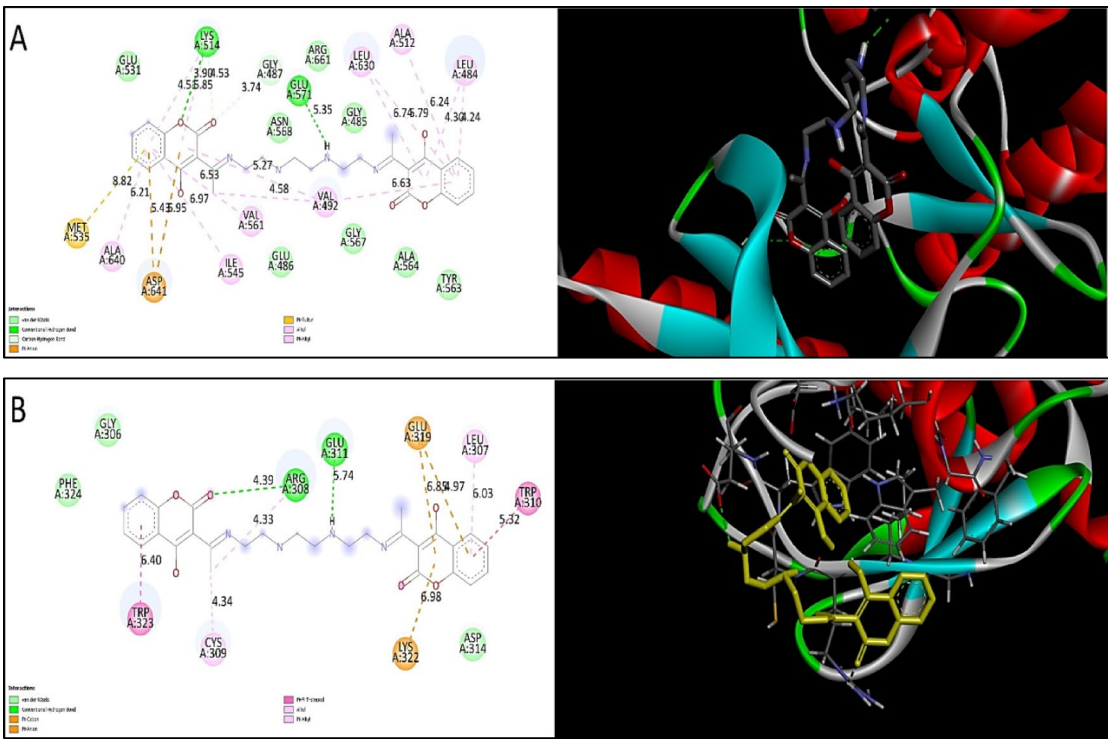



**Fig. 3**. 3D and 2D images of The binding model of compound 3c with (**A**) FGFR1 and (**B**) Anti-apoptotic protein (IAP). This figure was generated using the BIOVIA Discovery Studio 2024 v24.1.0.334.

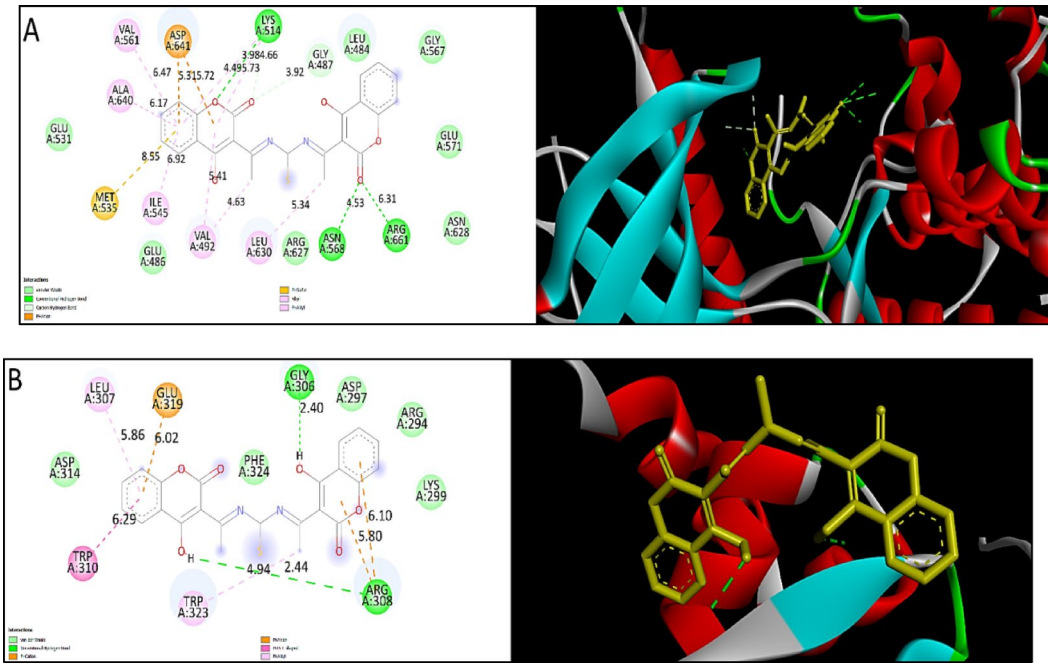



**Fig. 4**. 3D and 2D images of The binding model of compound 3f with (**A**) FGFR1 and (**B**) Anti-apoptotic protein (IAP). This figure was generated using the BIOVIA Discovery Studio 2024 v24.1.0.334.

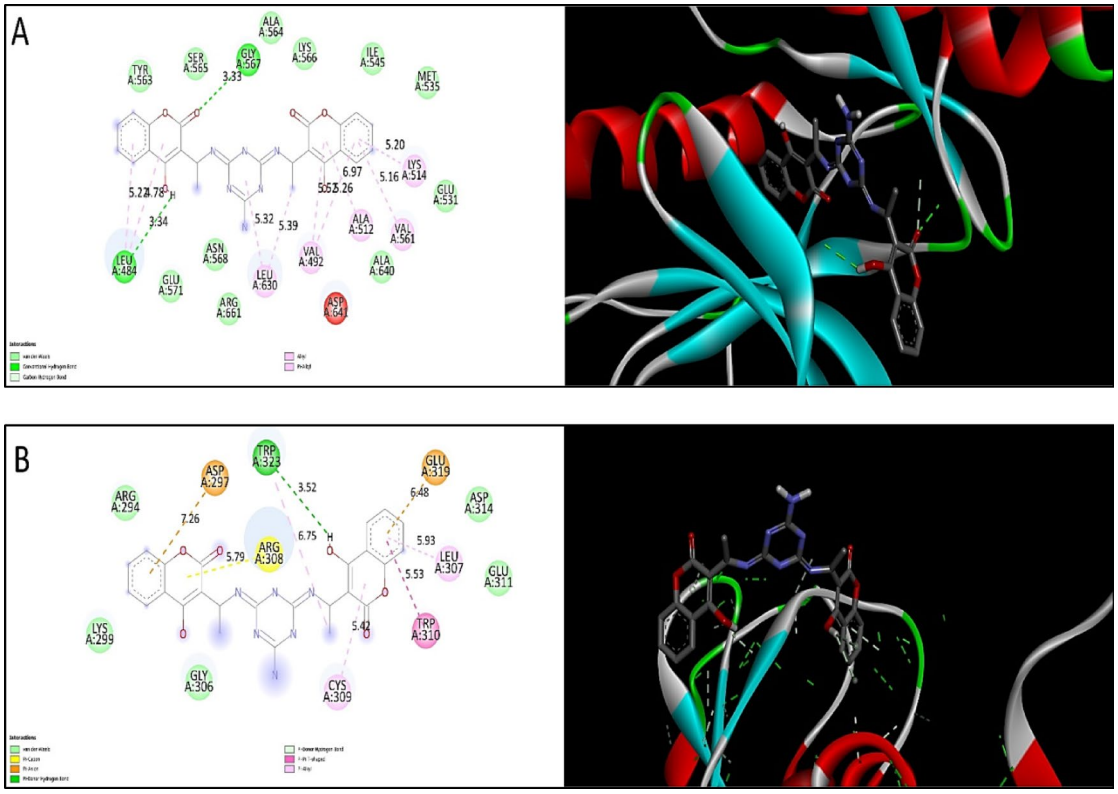



**Fig. 5**. 3D and 2D images of The binding model of compound 3j with (**A**) FGFR1 and (**B**) Anti-apoptotic protein (IAP). This figure was generated using the BIOVIA Discovery Studio 2024 v24.1.0.334.

| Compound | FGFR1 (3GQL) | cIAP1-BIR3 (4KMN) |
|---|---|---|
| **3b** (synthesized) | – 8.20 | – 6.00 |
| **3c** (synthesized) | – 7.70 | – 6.50 |
| **3f** (synthesized) | – 8.30 | – 7.20 |
| **3j** (synthesized) | – 9.50 | – 7.30 |
| **AZD4547** (*FGFR1* inhibitor) | – 11.2 to – 12.5 | N/A[56] |
| **PD173074** (*FGFR1* inhibitor) | – 10.8 to – 11.4 | N/A[57] |
| **Birinapant** (*cIAP1-BIR3* inhibitor) | N/A | -9.8 to -10.5[58] |
| **Tolinapant** (*cIAP1-BIR3* inhibitor) | N/A | -8.9 to -9.6[59] |

**Table 6**. Comparison of binding affinities of synthesized compounds with known *FGFR1* and *cIAP1-BIR3* Inhibitors. $IC_{50}$/Kd values were converted to ΔG using the van't Hoff equation (ΔG = RT·ln(Kd)).

exposure in the protein core. While the – 9.5 kcal/mol binding energy suggests strong affinity, the modest Rmsd value (1.764) hints at some conformational flexibility during binding, an observation that may inform future structural optimizations.

The *IAP* (4KMN) inhibition profile (Fig. 5B) presented a different interaction pattern, with compound **3j** adopting a distinct binding pose. Key features included: (i) a hydrogen bond (3.52 Å) between the coumarin oxygen and Trp323, (ii) two pi-anion interactions with Asp297/Glu319 that may contribute to binding specificity, and (iii) a mix of π-H and π-π interactions with residues lining the hydrophobic subpocket (particularly Trp310/323). The slightly reduced binding score (-7.30 kcal/mol) and higher Rmsd (5.062) versus *FGFR1* suggest that while compound **3j** effectively engages both targets, its *FGFR1* inhibition may be more conformationally constrained a finding that could prove significant for developing selective inhibitors.

The consistent pi-alkyl interactions observed between compounds **3b**, **3c**, **3f**, and **3j** and the amino acid residue Val492 in the *FGFR1* receptor (3GQL) shed light on the importance of specific molecular interactions in ligand binding. These interactions suggest that Val492 likely plays a crucial role in stabilizing ligand-receptor complexes at the active site of *FGFR1*. These findings underscore the complex interplay between ligand structure and receptor recognition.

The theoretical research suggests that compounds **3f** and **3j** have a robust and encouraging interaction with the *IAP* protein. This interaction inhibits the growth and metastasis by obstructing the tyrosine kinase domain of *IAP* through potent hydrogen bonding, thereby facilitating the apoptosis of cancer cells. The synthesized compound **3j** has the greatest binding affinity among the compounds tested, with a binding energy of -9.50 and – 7.30 kcal/mol, closely followed by **3f**, which has a binding score of -8.30 and – 7.20 kcal/mol.

Overall, compounds **3f** and **3j** appear to be the best inhibitor among the others, due to their strong binding affinity against both receptors and high degree of conformational match with the binding site, as indicated by the low RMSD value. Compound **3b** also shows strong interactions with *FGFR1*, but its interaction with *IAP* is less strong compared to compound **3f** and **3j**. Compound **3c** has a slightly weaker interaction with *FGFR1* and a slightly higher RMSD value compared to compound **3j**, indicating a slightly weaker binding affinity and a slightly lower degree of conformational match. These findings supported the results of the cytotoxic effectiveness that explained why compounds **3j** and **3f** displayed the highest effectiveness, especially against the *A549* cell line compare to the compounds **3b**, and **3c** and other synthesized compounds.

## Comparison of binding affinities and interaction profiles

To achieve a deeper insight into the binding affinities of the synthesized compounds to the *FGFR1* and *cIAP1-BIR3* proteins, comparative studies were performed in addition to the reported inhibitors of these proteins (Table 6). The comparative analysis allowed for an inclusive assessment of their efficacies individually.

***FGFR1*(3GQL Receptor)** Known *FGFR1* inhibitors (AZD4547, PD173074) interact strongly with Asn, Arg, and Lys residues via H-bonding and π-π stacking.

**Synthesized compounds:**

- **3b** interacts with Arg627, Lys514, Asn568 (H-donor and H-acceptor).
- **3c** interacts with Lys514, Glu571 (H-donor, H-acceptor).
- **3f** shows multiple H-bonding interactions with Arg661 and Asn568.
- **3j** interacts with Gly567 and Leu484, resembling interactions seen in *FGFR1* inhibitors.

***cIAP1-BIR3* (4KMN Receptor)**

Known *cIAP1* inhibitors (Birinapant, SM130, SM114) often target Trp, Arg, and Glu residues via H-bonding and π-π stacking.

**Synthesized compounds**:

- **3b** interacts with Glu311, Cys309, Trp323 (H-bonding).
- **3c** interacts with Glu311, Arg308, Trp310 (π-π stacking, H-bonding).
- **3f** interacts with Arg308, Gly306, Glu319 (H-bonding, π-cation).
- **3j** interacts with Trp323, Asp297, Glu319 (π-H, H-acceptor).

Our computational analysis reveals striking similarities between our compounds' binding modes and established *FGFR1/cIAP1* inhibitors, but with key advantages. While maintaining comparable binding affinities (**3j**: -9.5 kcal/mol vs. PD173074's -11.0 kcal/mol for *FGFR1*), our coumarin-based scaffolds achieve this through remarkably simplified chemistry.

The standout compound **3j** recapitulates critical interactions of clinical inhibitors: hydrogen bonds with *FGFR1*'s Lys514/Glu571 mirror PD173074's binding pattern, while its π-stacking with *cIAP1*'s Trp310 suggests rare dual-targeting capability. What makes this particularly exciting is that **3j** accomplishes this with a structure that's significantly more synthetically accessible than current therapeutic candidates.

These computational predictions position our compounds as promising candidates for targeted cancer therapy, particularly where dual inhibition of *FGFR1* and *cIAP1* pathways could prove advantageous.

The combination of simplified chemistry with sophisticated target engagement seen in compound **3j** could represent an important step toward more druggable *FGFR1/cIAP1* inhibitors.

### Structure-activity relationship (SAR) analysis

The analysis of the synthesized coumarin-based bisimines (**3a–j**) points to the existence of diverse structure–activity relationships pertaining to antibacterial, antifungal, and cytotoxic assessments. Among the evaluated derivatives, compound **3a** with the minimal hydrazine linker displayed the strongest antibacterial activity with MIC values equal to or greater than the reference drug controls, especially against *B. subtilis* and *S. aureus*. Such observation suggests that minimal alteration at the level of the imine nitrogen might enhance interactions with bacterial targets.

By contrast, compounds **3b** and **3c**, with methylated or extended aliphatic chains, showed higher cytotoxic activities ($IC_{50}$ ranging from 6 to 11 μM against *A549* and *MCF-7*) likely due to their increased lipophilicity, thus improving their ability to penetrate the membrane or interact with cancer-associated targets. Compound **3j**, with a melamine core, showed the lowest combined $IC_{50}$ values (5.58 μM for *A549*, 6.68 μM for *MCF-7*), a result consistent with its high binding affinity for both *FGFR1* and *cIAP1-BIR3* indicated by docking simulations, further pointing to a dual inhibitory action.

Interestingly, for the derivative **3f**, minimum inhibitory concentrations up to 1.95 μg/mL were recorded against *Penicillium verrucosum*, overtaking ketoconazole on various occasions. It might be surmised that the improved antifungal activity for **3f** is due to its ability to establish many hydrogen bonds that can account for both its structural behavior as well as the results of its docking research.

Overall, electron-donating substituents (e.g., **3b** and **3c**) seemed to enhance cytotoxicity, while hydrogen-bond-rich motifs (e.g., thiourea in **3f** and melamine in **3j**) exhibited a correlation between enhanced bioactivity. The structure-activity relationship (SAR) findings covered here provide a foundation for future rational design and optimization of coumarin-derived bisimines as multi-functional bioactives.

## Conclusion

In the realms of medicine and pharmaceuticals, Schiff bases have proven to be highly beneficial compounds. Their remarkable versatility, along with their antibacterial, antifungal, and anticancer properties, make them promising candidates for the development of novel therapeutic agents. The purpose of this investigation was to synthesize novel coumarin-derived Schiff bases through the reaction of 3-acetyl-4-hydroxycoumarin (2 mmol) with diamines (1 mmol) in MeOH, resulting in a favorable reaction rate and high yield of products. All the synthesized compounds were evaluated against Gram-negative bacteria such as *Escherichia coli* and *Pseudomonas aeruginosa*, and Gram-positive bacteria such as *Staphylococcus aureus* and *Bacillus subtilis*. Overall, compounds **3a-j** displayed antibacterial activities against Gram-positive and Gram-negative bacteria. The only compound that did not show any significant bacterial inhibition was compound **3f**. Based on the antibacterial activity measured against Gram-positive and Gram-negative bacteria, **3a** was found to be the most effective ($8.5 \pm 0.7$) and ($5.10 \pm 0.7$) against *E. coli* as Gram-negative and *S. aureus* as Gram-positive bacteria, respectively. The DPPH inhibitory potency of the synthesized compounds **3a-j** (70.2–96.7%) was satisfactory. The cytotoxic effects of the tested substances on *MCF-7*, *A549*, and *BEAS-2B* were also determined. The derivatives **3c** and **3f**, which incorporate thiourea and triethylenetetramine, were identified as the most potent cytotoxic agents, exhibiting characteristics comparable to doxorubicin in terms of their cytotoxic effects without any discernible selectivity. In contrast, the melamine analog **3j** was highlighted as a compound that, in terms of potency, matches doxorubicin but exhibits a superior selectivity profile. The coumarin Schiff base derivatives (**2**, **3b-c**, and **3j**) showed more prominent antioxidant activity (93.8, 96.7, and 94.1%) than other compounds. These observations could be explained by the fact that compounds **3b-c** and **3j** contain more polarizable nitrogen atoms (N) and more exchangeable protons (one $NH_2$ and two NH groups). According to findings from biological studies, synthesized bisimine derivatives have the potential to be highly effective antifungal agents. Furthermore, molecular docking was stimulated to study the bindings between the target proteins (PDB: 3GQL, and 4KMN) and the synthesized compounds. Moreover, analog **3j** demonstrated the best binding affinity against the active sites of 3GQL, and 4KMN compare to compounds **3c** and **3b**.

The inclusion of cIAP1-BIR3 and FGFR1 in the docking analysis was based on literature evidence of the overexpression of cIAP1 in various cancers and the structural similarity seen between key compounds (e.g., 3j and 3f) and known SMAC mimetics. The results of this docking analysis are intended to form the basis of hypothesis generation and highlight the potential for double inhibition mechanisms, which will be examined in more detail in future research efforts.

Based on the promising results obtained from the synthesis and biological assessment of novel coumarin Schiff bases, there are further avenues of research that can be explored to fully understand the potential applications and mechanisms of action of these compounds. By conducting mechanistic studies, evaluation of their cytotoxic

effects, in vivo investigations, formulation development, and clinical trials, a comprehensive understanding of these compounds' potential can be achieved.

## Data availability

The datasets used and/or analysed during the current study are available from the corresponding author on reasonable request.

Received: 23 April 2025; Accepted: 28 October 2025
Published online: 27 November 2025

## References

1. Baker, R. E. et al. Infectious disease in an era of global change. *Nat. Rev. Microbiol.* **20**, 193–205 (2022).
2. Simões, M., Bennett, R. N. & Rosa, E. A. Understanding antimicrobial activities of phytochemicals against multidrug resistant bacteria and biofilms. *Nat. Prod. Rep.* **26**, 746–757 (2009).
3. Mahapatra, M. et al. Coumaryl-sulfonamide moiety: unraveling their synthetic strategy and specificity toward *h* CA IX/XII, facilitating anticancer drug development. *Arch Pharm. (Weinheim)* **356**, (2023).
4. Min, S. J., Lee, H., Shin, M. S. & Lee, J. W. Synthesis and biological properties of pyranocoumarin derivatives as potent Anti-Inflammatory agents. *Int. J. Mol. Sci.* **24**, 10026 (2023).
5. Küpeli Akkol, E., Genç, Y., Karpuz, B., Sobarzo-Sánchez, E. & Capasso, R. Coumarins and Coumarin-Related compounds in pharmacotherapy of cancer. *Cancers (Basel).* **12**, 1959 (2020).
6. Alonso-Castro, A. J. et al. Antinociceptive, anti-inflammatory, and central nervous system (CNS) effects of the natural coumarin Soulattrolide. *Drug Dev. Res.* **79**, 332–338 (2018).
7. Chan, G. G., Koch, C. M. & Connors, L. H. Blood proteomic profiling in inherited (ATTRm) and acquired (ATTRwt) forms of Transthyretin-Associated cardiac amyloidosis. *J. Proteome Res.* **16**, 1659–1668 (2017).
8. Medina, F. G. et al. Coumarin heterocyclic derivatives: chemical synthesis and biological activity. *Nat. Prod. Rep.* **32**, 1472–1507 (2015).
9. Abdel-Latif, M. S., Elmeleigy, K. M., Aly, T. A. A., Khattab, M. S. & Mohamed, S. M. Pathological and biochemical evaluation of coumarin and chlorophyllin against aflatoxicosis in rat. *Exp. Toxicol. Pathol.* **69**, 285–291 (2017).
10. Kaur, J., Famta, P., Khurana, N., Vyas, M. & Khatik, G. L. Chapter 16 - Biomedical applications of 4-hydroxycoumarin as a fungal metabolite and its derivatives. in New and Future Developments in Microbial Biotechnology and Bioengineering (eds Singh, J. & Gehlot, P.) 209–218 (Elsevier, doi:https://doi.org/10.1016/B978-0-12-821006-2.00016-9. (2020).
11. Abdel Latif, N. A., Batran, R. Z., Khedr, M. A. & Abdalla, M. M. 3-Substituted-4-hydroxycoumarin as a new scaffold with potent CDK Inhibition and promising anticancer effect: Synthesis, molecular modeling and QSAR studies. *Bioorg. Chem.* **67**, 116–129 (2016).
12. Li, G. et al. Development of a series of 4-hydroxycoumarin platinum(IV) hybrids as antitumor agents: Synthesis, biological evaluation and action mechanism investigation. *J. Inorg. Biochem.* **194**, 34–43 (2019).
13. Srinivasan, R. et al. Antioxidant and Antiproliferative Potential of Bioactive Molecules Ursolic Acid and Thujone Isolated from *Memecylon edule* and *Elaeagnus indica* and Their Inhibitory Effect on Topoisomerase II by Molecular Docking Approach. *Biomed Res Int* 1–12 (2020). (2020).
14. Li, M. et al. Synthesis, crystal structures, and anti-drug-resistant Staphylococcus aureus activities of novel 4-hydroxycoumarin derivatives. *Eur. J. Pharmacol.* **721**, 151–157 (2013).
15. Hamdi, N., Fischmeister, C., Puerta, M. C. & Valerga, P. A rapid access to new coumarinyl chalcone and substituted chromeno[4,3-c] pyrazol-4(1H)-ones and their antibacterial and DPPH radical scavenging activities. *Med. Chem. Res.* **20**, 522–530 (2011).
16. Verma, M. et al. Antibacterial and antioxidant assay of novel heteroaryl-substituted methane derivatives synthesized via ceric ammonium nitrate (CAN) catalyzed one-pot green approach. *Mol. Divers.* **27**, 889–900 (2023).
17. Qin, W., Long, S., Panunzio, M. & Biondi, S. Schiff bases: A short survey on an evergreen chemistry tool. *Molecules* **18**, 12264–12289 (2013).
18. Liu, Y. et al. A Switch-On fluorescent probe for detection of mesotrione based on the straightforward cleavage of carbon-nitrogen double bond of schiff base. *Chem. Eng. J.* **430**, 132758 (2022).
19. Shirangi, H. S., Moradi, A. V., Golsefidi, M. A., Hossaini, Z. & Jalilian, H. R. Green synthesis and investigation of antioxidant and antimicrobial activity of new schiff base of Pyrimidoazepine derivatives: application of Fe3O4/CuO/ZnO@MWCNT MNCs as an efficient organometallic nanocatalyst. *Mol. Divers.* **26**, 3003–3019 (2022).
20. Pitchumani Violet Mary, C., Shankar, R. & Vijayakumar, S. Theoretical insights into the metal chelating and antimicrobial properties of the chalcone based schiff bases. *Mol. Simul.* **45**, 636–645 (2019).
21. Pandey, A., Rajavel, R., Chandraker, S. & Dash, D. Synthesis of schiff bases of 2-amino-5-aryl-1,3,4-thiadiazole and its Analgesic, Anti-Inflammatory and Anti-Bacterial activity. *E-J. Chem.* **9**, 145028 (2012).
22. Upadhyay, S. K. et al. In vitro Antitubercular Activity of Dihydropyridine-Dicarboxamide and Pyrazole Derivatives against *Mycobacterium tuberculosis*. *Bulletin of Pure & Applied Sciences- Zoology* 102https://doi.org/10.5958/2320-3188.2019.00011.1 (2019).
23. Dacrory, S., Hashem, A. H. & Hasanin, M. Synthesis of cellulose based amino acid functionalized nano-biocomplex: Characterization, antifungal activity, molecular Docking and hemocompatibility. *Environ. Nanotechnol Monit. Manag.* **15**, 100453 (2021).
24. Emami, S. & Dadashpour, S. Current developments of coumarin-based anti-cancer agents in medicinal chemistry. *Eur. J. Med. Chem.* **102**, 611–630 (2015).
25. Al-Amiery, A. A. Synthesis and antioxidant, antimicrobial evaluation, DFT studies of novel metal complexes derivate from schiff base. *Res. Chem. Intermed.* **38**, 745–759 (2012).
26. Branković, J. et al. Antioxidant and cytotoxic activities of selected Salicylidene imines: experimental and computational study. *Mol. Divers.* **26**, 3115–3128 (2022).
27. Emami, S. & Ghanbarimasir, Z. Recent advances of chroman-4-one derivatives: synthetic approaches and bioactivities. *Eur. J. Med. Chem.* **93**, 539–563 (2015).
28. Kotali, A. et al. Antioxidant activity of 3-[N-(Acylhydrazono)ethyl]-4-hydroxy-coumarins. *Molecules* **21**, (2016).
29. Batran, R. Z., Khedr, M. A., Abdel Latif, N. A., El Aty, A., Shehata, A. N. & A. A. & Synthesis, homology modeling, molecular docking, dynamics, and antifungal screening of new 4-hydroxycoumarin derivatives as potential chitinase inhibitors. *J. Mol. Struct.* **1180**, 260–271 (2019).
30. Bonardi, A. et al. Structural investigations on coumarins leading to chromeno[4,3-c]pyrazol-4-ones and pyrano[4,3-c]pyrazol-4-ones: new scaffolds for the design of the tumor-associated carbonic anhydrase isoforms IX and XII. *Eur. J. Med. Chem.* **146**, 47–59 (2018).
31. Wang, Z. C. et al. Sulfonamides containing coumarin moieties selectively and potently inhibit carbonic anhydrases II and IX: Design, synthesis, inhibitory activity and 3D-QSAR analysis. *Eur. J. Med. Chem.* **66**, 1–11 (2013).

32. Nawrot-Modranka, J., Nawrot, E. & Graczyk, J. In vivo antitumor, in vitro antibacterial activity and alkylating properties of phosphorohydrazine derivatives of coumarin and Chromone. *Eur. J. Med. Chem.* **41**, 1301–1309 (2006).
33. Brawley, J. et al. Synthesis and evaluation of 4-Hydroxycoumarin Imines as inhibitors of class II myosins. *J. Med. Chem.* **63**, 11131–11148 (2020).
34. Patil, S. A., Unki, S. N. & Badami, P. S. In vitro antibacterial, antifungal, and DNA cleavage studies of coumarin schiff bases and their metal complexes: synthesis and spectral characterization. *Med. Chem. Res.* **21**, 4017–4027 (2012).
35. Kalaiarasi, G., Jeya Rajkumar, S. R., Dharani, S., Małecki, J. G. & Prabhakaran, R. An investigation on 3-acetyl-7-methoxy-coumarin schiff bases and their Ru(< scp > ii) metallates with potent antiproliferative activity and enhanced LDH and NO release. *RSC Adv.* **8**, 1539–1561 (2018).
36. Erturk, A. G. Synthesis, structural identifications of bioactive two novel schiff bases. *J. Mol. Struct.* **1202**, 127299 (2020).
37. Vaseghi, S. et al. Synthesis, computational study and cytotoxicity of 4-hydroxycoumarin-derived imines/enamines. *Mol. Divers.* **25**, 1011–1024 (2021).
38. Olyaei, A. & Sadeghpour, M. Recent advances in the synthesis and biological activities of 3-aminoalkyl/3-amidoalkyl-4-hydroxycoumarin derivatives. *Synth. Commun.* **53**, 275–297 (2023).
39. Colombo, A. L., Barchiesi, F., McGough, D. A. & Rinaldi, M. G. Comparison of etest and National committee for clinical laboratory standards broth macrodilution method for Azole antifungal susceptibility testing. *J. Clin. Microbiol.* **33**, 535–540 (1995).
40. Salehi, P. et al. Synthesis of novel 1,2,3-triazole tethered 1,3-disubstituted β-carboline derivatives and their cytotoxic and antibacterial activities. *Med. Chem. Res.* **25**, 1895–1907 (2016).
41. Milella, R. A. et al. Correlation between antioxidant and anticancer activity and phenolic profile of new Apulian table grape genotypes (V. Vinifera L). *Front Plant. Sci* **13**, (2023).
42. Espinel-Ingroff, A., Canton, E., Peman, J. & Martín-Mazuelo, E. Comparison of Anidulafungin mics determined by the clinical and laboratory standards Institute broth microdilution method (M27-A3 Document) and etest for *Candida* species isolates. *Antimicrob. Agents Chemother.* **54**, 1347–1350 (2010).
43. van Meerloo, J., Kaspers, G. J. L. & Cloos, J. Cell sensitivity assays: the MTT assay. in 237–245 (2011). https://doi.org/10.1007/978-1-61779-080-5_20
44. Tokalı, F. S., Şenol, H., Bulut, Ş. & Hacıosmanoğlu-Aldoğan, E. Synthesis, characterization and molecular Docking studies of highly selective new hydrazone derivatives of anthranilic acid and their ring closure analogue Quinazolin-4(3H)-ones against lung cancer cells A549. *J. Mol. Struct.* **1282**, 135176 (2023).
45. Bae, J. H. et al. The selectivity of receptor tyrosine kinase signaling is controlled by a secondary SH2 domain binding site. *Cell* **138**, 514–524 (2009).
46. Dai, S., Zhou, Z., Chen, Z., Xu, G. & Chen, Y. Fibroblast growth factor receptors (FGFRs): structures and small molecule inhibitors. *Cells* **8**, 614 (2019).
47. Stadlbauers, W. & Hojas, G. Ring closure reactions of 3-arylhydrazonoalkyl-quinolin-2-ones to 1-aryl-pyrazolo[4,3- *c* ]quinolin-2-ones. *J. Heterocycl. Chem.* **41**, 681–690 (2004).
48. Gulcin, İ. & Alwasel, S. H. DPPH radical scavenging assay. *Processes* **11**, 2248 (2023).
49. Sumrra, S. H. et al. Metal incorporated sulfonamides as promising multidrug targets: combined enzyme inhibitory, antimicrobial, antioxidant and theoretical exploration. *J. Mol. Struct.* **1250**, 131710 (2022).
50. Abumelha, H. M. et al. Molecular modeling of new thiazolyl-thiophene based compounds as antioxidant agents. *J. Mol. Struct.* **1262**, 133112 (2022).
51. Zheng, Y. et al. Novel Mandelic acid derivatives containing piperazinyls as potential candidate fungicides against monilinia fructicola: Design, synthesis and mechanism study. *Bioorg. Chem.* **151**, 107647 (2024).
52. Bareth, D. et al. Synthetic and Pharmacological developments in the hybrid s-triazine moiety: A review. *Bioorg. Chem.* **143**, 106971 (2024).
53. Zhou, R., Yu, Y. H., Kim, H. & Ha, H. H. Synthesis of coumarin derivatives and investigation of their inhibitory effects on lung cancer cell motility. *Sci. Rep.* **12**, 21635 (2022).
54. Wang, Y. et al. Discovery and characterization of novel FGFR1 inhibitors in triple-negative breast cancer via hybrid virtual screening and molecular dynamics simulations. *Bioorg. Chem.* **150**, 107553 (2024).
55. Fathi, E. M. et al. Design, Synthesis, In silico and In Vitro Anticancer Activity of Novel Bis-Furanyl-Chalcone Derivatives Linked through Alkyl Spacers. *ChemistrySelect* 6, 6202–6211 (2021).
56. Dai, A. Future warming patterns linked to today's climate variability. *Sci. Rep.* **6**, 19110 (2016).
57. Akkachairin, B. et al. Synthesis of neocryptolepines and carbocycle-fused Quinolines and evaluation of their anticancer and antiplasmodial activities. *Bioorg. Chem.* **98**, 103732 (2020).
58. Dixon, S. J. et al. Human haploid cell genetics reveals roles for lipid metabolism genes in nonapoptotic cell death. *ACS Chem. Biol.* **10**, 1604–1609 (2015).
59. Wang, Y. et al. Genome-wide screens identify Toxoplasma gondii determinants of parasite fitness in IFNγ-activated murine macrophages. *Nat. Commun.* **11**, 5258 (2020).


## Acknowledgements

In particular, the University of Mazandaran's Research Council deserves special appreciation for supporting this research.

## Author contributions

***A. Abazari***:*** Investigation ***,*** Writing – original draft, Formal analysis.***Y. Sarrafi: *** Validation, Writing – review and editing.***P. Taheri: *** Software, Writing – original draft, Writing – review and editing, Formal analysis.***M. Tajbakhsh: *** Conceptualization, Project administration, Supervision.

## Declarations

## Competing interests

The authors declare no competing interests.

## Additional information

**Supplementary Information** The online version contains supplementary material available at https://doi.org/10.1038/s41598-025-26301-9.

**Correspondence** and requests for materials should be addressed to P.T.

**Reprints and permissions information** is available at www.nature.com/reprints.

**Publisher's note** Springer Nature remains neutral with regard to jurisdictional claims in published maps and institutional affiliations.

**Open Access** This article is licensed under a Creative Commons Attribution-NonCommercial-NoDerivatives 4.0 International License, which permits any non-commercial use, sharing, distribution and reproduction in any medium or format, as long as you give appropriate credit to the original author(s) and the source, provide a link to the Creative Commons licence, and indicate if you modified the licensed material. You do not have permission under this licence to share adapted material derived from this article or parts of it. The images or other third party material in this article are included in the article's Creative Commons licence, unless indicated otherwise in a credit line to the material. If material is not included in the article's Creative Commons licence and your intended use is not permitted by statutory regulation or exceeds the permitted use, you will need to obtain permission directly from the copyright holder. To view a copy of this licence, visit http://creativecommons.org/licenses/by-nc-nd/4.0/.

© The Author(s) 2025